
TÜRKİYE CUMHURİYETİ'NİN YÜZÜNCÜ YILI
Uzaktan Konumsal
Araştırma ve Analiz
Editör
Fazıl Nacar
BİDGE

BIDGE Publications

Uzaktan Konumsal Araştırma ve Analiz

Editor: Doç. Dr. Fazıl Nacar

ISBN: 978-625-372-268-5

Page Layout: Gözde YÜCEL

1st Edition:

Publication Date: 25.06.2024

BIDGE Publications,

www.bidgeyayinlari.com.tr - bidgeyayinlari@gmail.com

Krc Bilişim Ticaret ve Organizasyon Ltd. Şti.
Güzeltepe Mahallesi Abidin Daver Sokak Sefer Apartmanı No: 7/9 Çankaya / Ankara

Content

Drought Analysis Using SPI and SPEI Methods in the Ermenek Dam Basin 4

Cafer Tayyar OKKA 4

Süleyman Savaş DURDURAN 4

Tansu ALKAN, ... 4

Spatial Analysis of Culicoides Biting Midges (Diptera: Ceratopogonidae) in the Western Black Sea Region 31

Ilkay BUGDAYCI 31

Melike GOKCE 31

Trend Analysis of Temperature and Precipitation in Ermenek Dam Basin 57

Süleyman Savaş DURDURAN 57

Cafer Tayyar OKKA 57

Tansu ALKAN, ... 57

Türkiye'deki Ormanlık Alanlardaki 20 Yıllık Değişimin Google Earth Engine ile İzlenmesi: 2001-2021 Analizi 89

Duygu ARIKAN 89

Ferruh YILDIZ 89

CHAPTER I

Drought Analysis Using SPI and SPEI Methods in the Ermenek Dam Basin

Cafer Tayyar OKKA[1]
Süleyman Savaş DURDURAN[2]
Tansu ALKAN[3,4]

Introduction

Climate change induced by global warming represents a substantial challenge for both society and ecosystems. The consequential impact of climate change is evident in the escalating occurrences of water scarcity and drought events, giving rise to a multitude of socioeconomic issues. Drought, characterized as a natural disaster, exhibits a highly intricate structure and stands out as one of the meteorologically rooted calamities with profound

[1] State Hydraulic Works 4th Regional Directorate, Konya, Orcid: 0000-0001-8338-8431
[2] Necmettin Erbakan University, Department of Geomatics Engineering, Konya, Orcid: 0000-0003-0509-4037
[3] Niğde Ömer Halisdemir University, Department of Geomatics Engineering, Niğde, Orcid: 0000-0001-8293-2765
[4] Necmettin Erbakan University, Institute of Science, Konya

negative implications for human life (Ashraf & Routray, 2013). Unlike other natural disasters, drought unfolds gradually but exerts its influence over an extended timeframe and extensive geographical areas. It is defined as a substantial reduction in precipitation below the average levels during any season or temporal span. The severity of drought is exacerbated by additional climatic factors such as elevated temperatures, heightened wind speeds, and diminished humidity (Sırdaş & Şen, 2003; Chen, Kuo & Yu, 2009; Fontaine & Steinemann, 2009; Bacanlı & Kargı, 2019). The repercussions of drought extend beyond the depletion of surface water bodies like rivers, dams, and lakes to encompass groundwater, resulting in water scarcity, increased susceptibility to epidemics, reduced agricultural output, and a decline in hydroelectric power generation (Arslan, Bilgil & Veske, 2016).

Drought is classified into four distinct categories: meteorological drought, agricultural drought, hydrological drought, and socioeconomic drought. Meteorological drought, the initial phase, is characterized by reduced precipitation compared to the established average over a specific period (Anisfeld, 2011; Aktürk, Zeybekoğlu & Yıldız, 2022). Subsequently, agricultural drought ensues, signifying insufficient soil moisture for optimal plant growth. Hydrological drought arises from the prolonged persistence of meteorological and agricultural droughts (Taylan & Bahşi, 2021), representing a subpar reduction in water resources. Socioeconomic drought encompasses adverse impacts on social and economic facets of life.

Several indices have been devised to gauge and monitor drought, offering a simplified understanding of intricate

relationships within climatic parameters and processes (Akbaş, 2014). These indices facilitate the quantitative assessment of drought events concerning location, timing, and duration (Menteşe & Akbulut, 2023). Input data for these indices encompass various parameters such as temperature, potential evapotranspiration, evapotranspiration, wind speed, and notably, precipitation. The Standardized Precipitation Index (SPI) and Standardized Precipitation Evapotranspiration Index (SPEI) are widely employed in the literature due to their efficacy in capturing drought characteristics, including severity and duration (Aktürk, Zeybekoğlu & Yıldız, 2022). SPI delineates wet and dry periods based solely on precipitation, while SPEI incorporates both precipitation and potential evapotranspiration, designed specifically for analyzing agricultural drought severity (Bakanoğulları, 2020). The outcomes of drought analyses are pivotal for water resource management, formulation of drought action plans, and the implementation of drought-related measures.

In the scholarly literature, investigations into drought analysis employing the SPI have been undertaken across various geographical locations, including Romania (Ionita, Scholz & Chelcea, 2016), Europe, and the Mediterranean Basin (Caloiero & et al., 2018), Çanakkale (Ilgar, 2010), Seyfe Lake (Kıymaz, Güneş & Asar, 2011), Van Lake Basin (Yetmen, 2013), Kızılırmak Basin (Arslan, Bilgil & Veske, 2016), Bilecik (Karaer & Gültaş, 2018), Bursa (Bacanlı & Kargı, 2019), Çorak Lake Basin (Şener & Şener, 2019), Isparta (Uçar, Topçu & Demirel, 2019), Gaziantep (Taylan & Bahşi, 2021), Konya Closed Basin (Sarış & Gedik, 2021), Şanlıurfa (İrcan & Duman, 2021), and the Bilecik Merkez and Bozüyük districts (Menteşe & Akbulut, 2023). Similarly, the SPEI has been

employed to investigate drought occurrences in the Haihe River Basin of China (Yang & et al., 2016), South Korea (Bae & et al., 2018), and the Meric River Basin (Erişmiş, 2023). Concurrently, joint analyses utilizing both SPI and SPEI methods have been conducted in diverse regions, such as the Kafue Basin in northern Zambia (Tirivarombo, Osupile & Eliasson, 2018), Ankara (Danandeh Mehr & Vaheddoost, 2020), Kumdere Basin (Bakanoğulları, 2020), Inner Mongolia region of China (Pei & et al., 2020), Bangladesh (Kamruzzaman & et al., 2022), Samsun (Yüce & et al., 2022), and Kırıkkale (Aktürk, Zeybekoğlu & Yıldız, 2022). Furthermore, distinct indices, namely SPI, Precipitation Anomaly Index, and Percentage of Normal Precipitation Index, were utilized in Isparta (Şener & Davraz, 2021), SPI and Chinese Z index in the Burdur Lake Basin (Şener & Şener, 2021), and SPEI and Integrated Drought Index in Erzurum (Topçu & Karaçor, 2021), facilitating a comparative assessment of different indices in the context of drought analysis.

This study contributes to the literature by investigating in which direction drought is affected in the transition regions from Mediterranean climate to continental climate. Within the scope of this investigation, an examination of drought conditions was conducted in the Ermenek Dam Basin employing the SPI and the SPEI methodologies. SPI and SPEI values were computed for varying temporal scales, specifically, 1, 3, 6, 12, and 24-month periods, utilizing meteorological data spanning from 1980 to 2021 obtained from monitoring stations in Alanya, Anamur, Karaman, Konya, and Seydişehir. Upon scrutinizing the resultant values, it is deduced that the basin is predominantly characterized by normal and

near-normal dry conditions, indicative of a proclivity towards drought within the basin.

Material and method

Material

Ermenek is situated within the Karaman province, positioned in the southern region of Anatolia. This district, distinguished by its mountainous topography, shares boundaries with the Hadim district of the Konya province and the Central District of the Karaman province to the north. To the south, it is adjacent to the Anamur district of the Mersin province and the Gazipaşa district of the Antalya province. In the east, Ermenek is bordered by the Gülnar and Mut districts of the Mersin province, while in the west, it shares borders with the Sarıveliler and Başyayla districts of the Karaman province. The district spans an approximate surface area of 1,223 km^2. The climate in Ermenek exhibits characteristics that lie within the transitional zone between a continental and Mediterranean climate. However, the Mediterranean climate features are more prevalent. The region is predominantly mountainous, lacking extensive plains, though agricultural activities can be undertaken in the plains situated between the valleys.

The research aimed to conduct a drought analysis in the Ermenek Dam Basin (Figure 1), utilizing data from Alanya, Anamur, Ermenek, Karaman, and Mut stations. However, it was not feasible to incorporate data from the Ermenek and Mut stations due to specific circumstances. The Ermenek station, for instance, underwent closure in 2004, only to be reopened in 2013. Conversely, the Mut station exhibited data gaps, notably during the period between 1986 and 1993 and in various intermittent periods.

Consequently, Konya and Seydişehir stations were included as substitutes in the analysis. The dataset, sourced from the General Directorate of Meteorology and State Hydraulic Works, spans a temporal range of 498 months, commencing from January 1980 and concluding in June 2021. Subsequently, SPI and SPEI values were computed across intervals of 1, 3, 6, 12, and 24 months. The data was distributed using the Chi-squared test before calculating SPI and SPEI values. The indices were then calculated using Excel based on the calendar year. Table 1 presents the average, maximum, standard deviation, the lagged autocorrelation coefficient, kurtosis, and skewness of the monthly precipitation data for the stations.

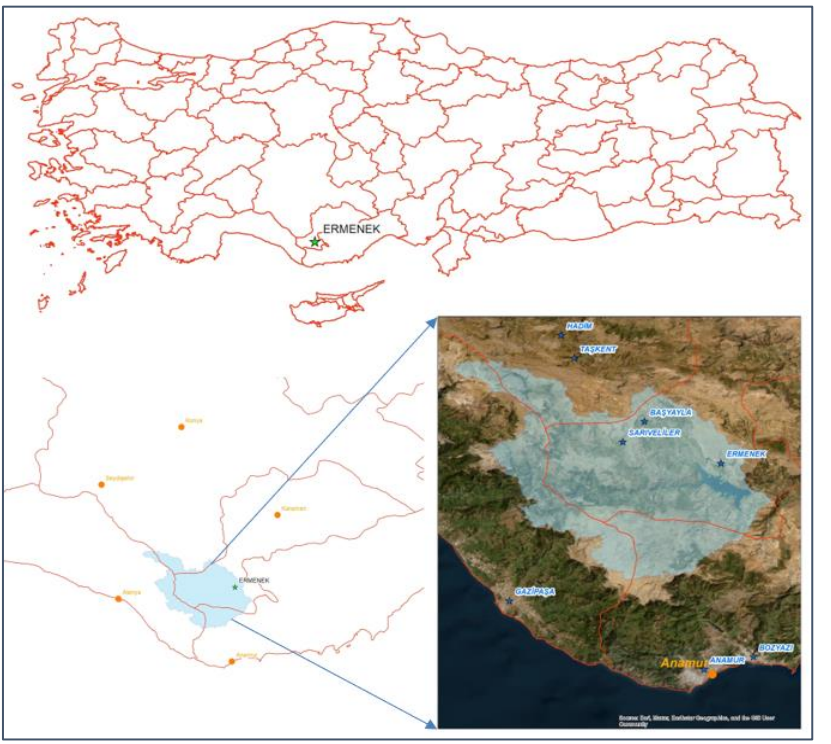

Figure 1: Ermenek dam basin

Ermenek District is situated in the transition zone between the continental and Mediterranean climates. The district center is approximately 1250 m above sea level. The average precipitation in the district center was 527.3 mm/year between 1950-2004, but decreased to 425.9 mm/year after 2013. Temperature values show an increase from 12.4 ℃ (measured between 1965 and 2004) to 13 ℃ (measured after 2013).

Table 1: Descriptive statistics for the stations

Stations	Average	Maximum	Standard deviation	The lagged autocorrelation coefficient	Kurtosis	Skewness
Alanya	93,16	710,40	114,05	0,44	4,87	1,91
Anamur	75,92	590,90	97,41	0,48	3,52	1,74
Karaman	27,00	175,00	24,18	0,22	2,77	1,23
Konya	26,91	124,00	24,08	0,16	1,51	1,20
Seydişehir	63,67	487,40	66,06	0,35	6,77	2,04

Method

Swed-Eisenhart (run) test

Run test is a non-parametric test used to verify that the data in a time series are independent of each other and originate from the same population (Aktürk, Zeybekoğlu & Yıldız, 2022). This test checks the homogeneity of the data based on the assumptions of H_0 (homogeneous) or H_1 (not homogeneous). The homogeneity of the data is determined by the Z value given in Equation (1).

$$Z = \frac{r - \frac{N_a N_b}{N_a + N_b} + 1}{\sqrt{\frac{2N_a N_b (2N_a N_b - N)}{N^2 (N-1)}}} \quad (1)$$

The equation defines Z as the test result, N as the number of data, r as the number of runs, N_a as the number of values less than the median value of the series, and N_b as the number of values greater

than the median. If the obtained Z value falls between ±1,96, the data is homogeneously distributed within the 95% confidence interval, and the null hypothesis (H_0) is accepted. Otherwise, the alternative hypothesis (H_1) is accepted (Swed & Eisenhart, 1943).

Run test results of the stations are given in Table 2.

Table 2: Run test results

	Alanya	Anamur	Karaman	Konya	Seydişehir
Median	53,95	33,20	23,75	20,95	45,10
r	128	124	193	213	173
N	498	498	498	498	498
N_a	249	249	249	249	248
N_b	249	249	249	249	250
Z	-10,95	-11,30	-5,11	-3,32	-6,91

Hypothesis H_1 is accepted based on the Z values.

Standardized precipitation index (SPI)

The SPI, extensively employed in drought analysis, was formulated by McKee et al. (1993). A key strength of this approach lies in its flexibility, allowing for the utilization of diverse time scales in assessing the impact of drought on ground and surface water reservoirs, as well as agricultural activities in response to precipitation deficiencies (Yetmen, 2013). Precipitation constitutes the primary meteorological data utilized within the SPI method. Typically, SPI values are computed across time scales of 3, 6, 9, 12, 24, and 48 months. Short-term intervals furnish crucial insights into water potential and agricultural water demand, whereas longer-term periods offer significant information pertinent to groundwater investigations and the management of water resources (Mishra & Singh, 2011; Şener & Davraz 2021). Notably, a minimum of 30 years' worth of precipitation data is requisite for the application of this method (İrcan & Duman, 2021).

SPI is calculated with Equation (2).

$$SPI = \frac{X_i - X_{avg}}{\sigma} \quad (2)$$

Given in Equation (2), X_i refers to total precipitation for a given period, X_{avg} refers to the average total precipitation for the same period and σ refers to the standard deviation. Periods when the SPI value is above zero are considered as wet periods, while periods when it is below zero are considered as dry periods. The time period when SPI values are continuously negative is called dry period.

Standardized precipitation evapotranspiration index (SPEI)

The SPEI represents an extension of the widely adopted SPI (Yüce & et al., 2022), and it was formulated by Vicente-Serrano et al. (2010). In this method, data pertaining to potential evapotranspiration (PET), derived from both precipitation and temperature parameters, is employed. SPEI is computed by utilizing the disparity between precipitation (P) and PET (Equation (3)) as an input condition (Tirivarombo, Osupile & Eliasson, 2018).

$$D_i = P_i - PET_i \quad (3)$$

Given in the Equation (3), D_i refers to water surplus or deficit in the analyzed month, P_i refers to precipitation and PET_i refers to potential evapotranspiration. In this study, PET values were calculated using the Thornthwaite (1948) model (Equation (4-7)).

$$i = \left(\frac{t}{5}\right)^{1.514} \quad (4)$$

$$I = \sum_1^{12} i \quad (5)$$

$$PET = 16 * \left(\frac{10 * t}{I}\right)^{a} * G \quad (6)$$

$$a = (6.7510 * 10^{-7} * I^3) - (7.7110 * 10^{-5} * I^2) + (1.791210 * 10^{-2} * I) + 0.49239 \quad (7)$$

Given in the Equation (4-7), i refers to monthly temperature index, t refers to average monthly temperature, I refers to annual temperature index, a refers to a parameter and G refers to the latitude correction coefficient.

The classification of SPI and SPEI values is given in Table 3.

Table 3: Classification of SPI and SPEI values

Drought Class	SPI / SPEI Values
Extremely wet (EW)	≥ 2
Very wet (VW)	1,50 ~ 1,99
Moderately wet (MW)	1,00 ~ 1,49
Normal (N)	0 ~ 0,99
Near normal dry (NND)	-0,99 ~ 0
Moderately dry (MD)	-1,00 ~ -1,49
Very dry (VD)	-1,50 ~ -1,99
Extremely dry (ED)	≤ -2

Results

This investigation involved the computation of SPI and SPEI values based on data collected from Alanya, Anamur, Karaman, Konya, and Seydişehir stations. The aim was to analyze drought occurrences within the Ermenek Dam Basin spanning the period from 1980 to 2021. The outcomes derived from these analyses were subsequently assessed on a station-specific basis.

Alanya station

The results of SPI and SPEI indices obtained using Alanya station data are given in Table 4.

Table 4: Number of drought severity at different time scales at Alanya station

Class	Index	1 Month	3 Month	6 Month	12 Month	24 Month
EW	SPI/SPEI	26/10	23/10	18/8	21/2	14/1
VW	SPI/SPEI	14/29	26/26	28/28	15/38	11/33
MW	SPI/SPEI	21/49	33/55	32/50	51/43	47/53
N	SPI/SPEI	125/167	132/156	151/166	136/162	160/164
NND	SPI/SPEI	269/160	226/165	188/151	178/153	156/126
MD	SPI/SPEI	38/55	52/59	68/65	67/64	46/69
VD	SPI/SPEI	5/23	3/21	7/20	17/22	39/28
ED	SPI/SPEI	0/1	1/4	1/5	2/3	2/1

At the Alanya station, within the SPI values computed based on 12-month data, 223 months exhibited wet conditions, while 264 months indicated dry conditions. Correspondingly, in the SPEI values, 245 months were characterized by wet conditions, and 242 months exhibited dry conditions. For SPI values calculated over a 24-month period, 232 months were wet, and 243 months were dry. In contrast, SPEI values for the same period showed 251 months with wet conditions and 224 months with dry conditions. Commencing from December 2003, the lengthiest uninterrupted dry spell was 69 months for SPI and 73 months for SPEI. In SPEI values, during the 61-month period starting in January 2014, there was an escalation in the number of months categorized as moderately dry and very dry, indicating an intensification of dry conditions. The most protracted wet phase occurred over 52 months since September 2009 for SPI and an extended period of 107 months since December 1981 for SPEI. Graphical representations of SPI and SPEI indices before and after the year 2000 are presented in Figure 2.

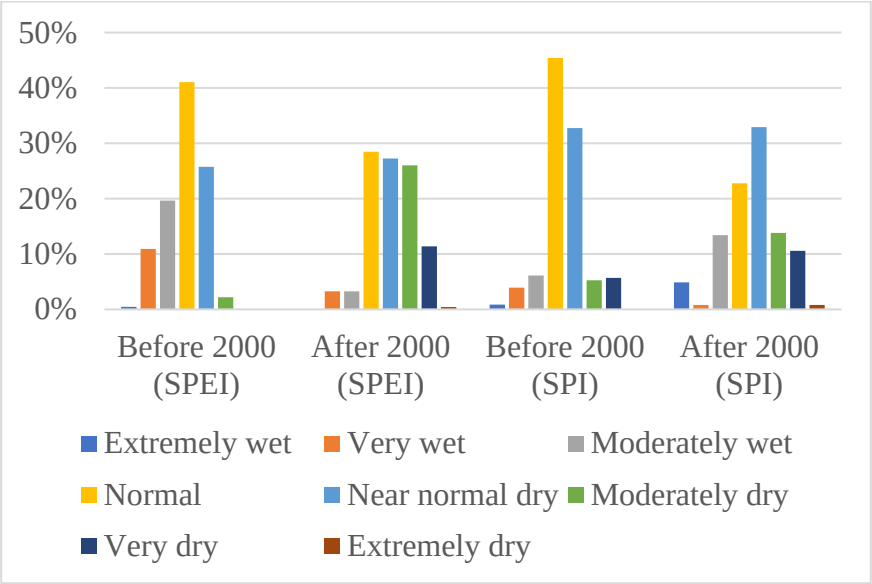

Figure 2: SPI and SPEI values of Alanya station before and after 2000

Upon scrutinizing Figure 2, it is observed that, in accordance with the SPI values, precipitation exhibited moderate and normal wet patterns before the year 2000. However, post-2000, there is a discernible shift towards moderate and very wet conditions. Notably, a gradual increase in dry conditions is evident after the year 2000.

Anamur station

The results of SPI and SPEI indices obtained using Anamur station data are given in Table 5.

Table 5: Number of drought severity at different time scales at Anamur station

Class	Index	1 Month	3 Month	6 Month	12 Month	24 Month
EW	SPI/SPEI	23/10	24/8	22/8	24/8	8/0
VW	SPI/SPEI	14/26	22/30	17/22	14/31	32/28
MW	SPI/SPEI	27/50	23/48	38/64	36/41	47/65
N	SPI/SPEI	121/169	150/160	155/145	168/174	143/148
NND	SPI/SPEI	271/162	214/165	188/178	178/149	169/132
MD	SPI/SPEI	38/52	53/56	56/45	42/52	52/75
VD	SPI/SPEI	4/25	9/24	12/23	11/21	22/27
ED	SPI/SPEI	0/4	1/5	5/8	14/11	2/0

At the Anamur station, the analysis of SPI values derived from 12-month data revealed 242 months with wet conditions and 245 months with dry conditions, whereas SPEI values indicated 254 months with wet conditions and 233 months with dry conditions. For SPI values calculated over a 24-month period, 230 months were wet, and 245 months were dry, while SPEI values showed 241 months with wet conditions and 234 months with dry conditions. The lengthiest uninterrupted dry period observed was 89 months in SPI values since April 1989 and 72 months in SPEI values since March 1990. During the 60-month period commencing in 2014, there was an escalation in the number of months characterized by moderately dry and very dry conditions, indicating an intensification of dry conditions in SPEI values. Conversely, the most protracted wet phase recorded is 60 months in SPI values since February 2009 and 59 months in SPEI values since December 1981. Graphical representations of SPI and SPEI indices before and after the year 2000 are presented in Figure 3.

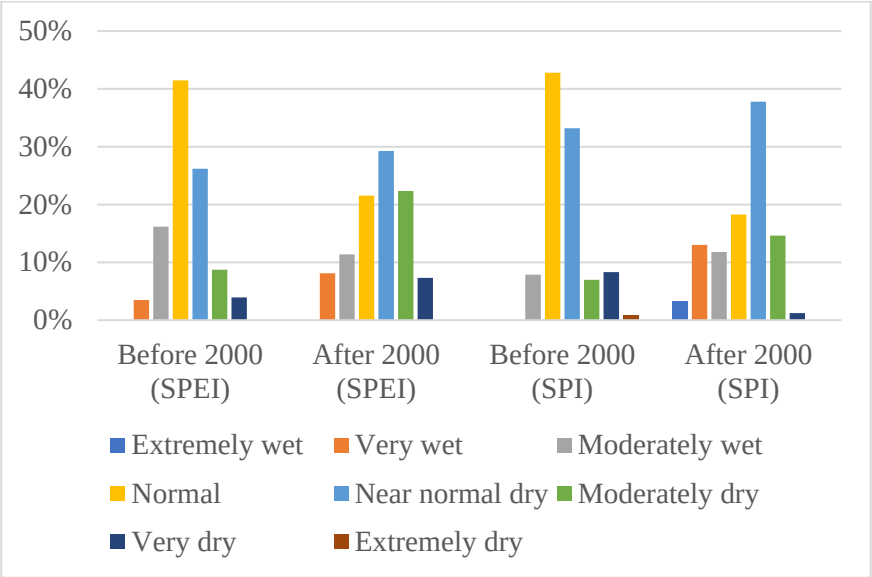

Figure 3: SPI and SPEI values of Anamur station before and after 2000

Upon examination of Figure 3, it is discerned that, based on SPI values, conditions characterized as wet were moderately wet and normal before the year 2000, transitioning to moderately wet and very wet after 2000. Prior to 2000, the dry period gave way to a wet period. In terms of SPEI values, a predominance of wet conditions is evident before 2000, yet the impact of wetness diminishes while the severity of dry conditions intensifies post-2000.

Karaman station

The results of SPI and SPEI indices obtained using Karaman station data are given in Table 6.

Table 6: Number of drought severity at different time scales at Karaman station

Class	Index	1 Month	3 Month	6 Month	12 Month	24 Month
EW	SPI/SPEI	23/7	18/8	19/8	19/8	13/2
VW	SPI/SPEI	20/31	27/22	17/24	29/22	28/39
MW	SPI/SPEI	37/49	36/64	44/58	33/59	39/52
N	SPI/SPEI	118/160	143/151	156/163	141/157	143/136
NND	SPI/SPEI	244/163	202/165	174/156	196/154	177/173
MD	SPI/SPEI	49/56	54/58	57/54	48/60	53/43
VD	SPI/SPEI	5/30	15/19	23/23	19/22	16/21
ED	SPI/SPEI	2/2	1/9	3/7	2/5	6/9

At the Karaman station, the analysis of SPI values derived from 12-month data revealed 222 months with wet conditions and 265 months with dry conditions, while corresponding SPEI values indicated 246 months with wet conditions and 241 months with dry conditions. For SPI values calculated over a 24-month period, 223 months were wet, and 252 months were dry, while SPEI values showed 229 months with wet conditions and 246 months with dry conditions. The most extended uninterrupted dry period observed was 62 months, commencing from February 2005 in SPI values, and 83 months, starting from March 2005 in SPEI values. According to SPEI values, there is an increase in the number of months characterized by moderately dry and very dry conditions, resulting in a more pronounced dry trend. Conversely, the lengthiest wet phase recorded is 77 months since November 2014 for SPI values and 40 months since December 1981 for SPEI values. Graphical representations analyzing SPI and SPEI indices before and after the year 2000 are presented in Figure 4.

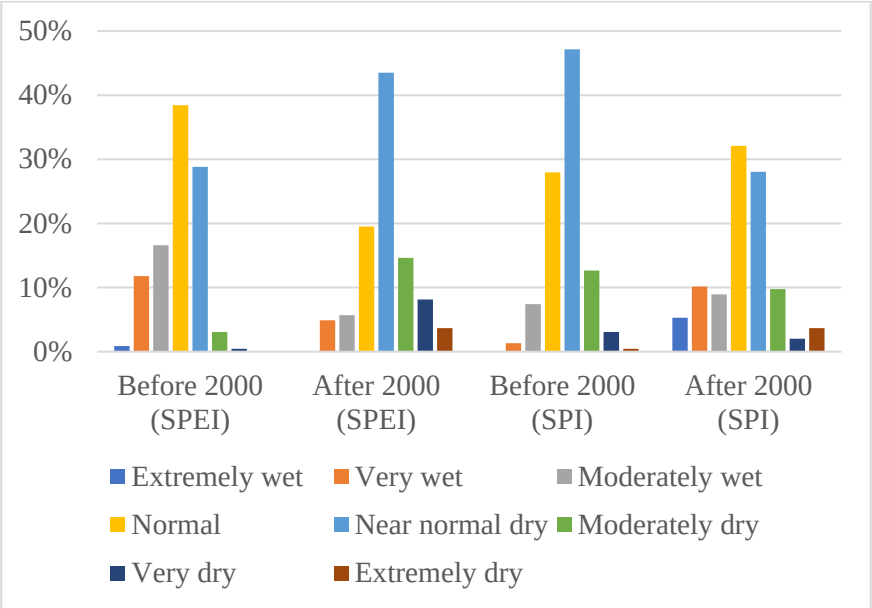

Figure 4: SPI and SPEI values of Karaman station before and after 2000

Upon examination of Figure 4, it is evident that, based on SPI values, the Karaman station, despite exhibiting continental climate characteristics before the year 2000, persisted in a wet period after 2000. Of the 246 months calculated, 139 were categorized as normal and wet. In terms of SPEI values, the prevalence of wet conditions was notable before 2000. However, post-2000, there is a discernible reduction in the impact of wetness, accompanied by an escalation in the severity of dry conditions.

Konya station

The results of SPI and SPEI indices obtained using Konya station data are given in Table 7.

Table 7: Number of drought severity at different time scales at Konya station

Class	Index	1 Month	3 Month	6 Month	12 Month	24 Month
EW	SPI/SPEI	27/10	13/7	15/9	18/2	4/1
VW	SPI/SPEI	20/18	28/26	18/24	14/37	21/32
MW	SPI/SPEI	27/61	42/55	35/47	27/47	57/64
N	SPI/SPEI	131/158	155/160	176/170	196/158	154/140
NND	SPI/SPEI	239/167	184/171	167/157	145/160	156/154
MD	SPI/SPEI	47/57	54/48	50/55	55/57	46/56
VD	SPI/SPEI	7/21	17/21	30/21	30/20	30/26
ED	SPI/SPEI	0/6	3/8	2/10	2/6	7/2

At the Konya station, the analysis of SPI values derived from 12-month data revealed 255 months with wet conditions and 232 months with dry conditions, while corresponding SPEI values indicated 244 months with wet conditions and 243 months with dry conditions. For SPI values calculated over a 24-month period, 236 months were wet, and 239 months were dry, while SPEI values showed 237 months with wet conditions and 238 months with dry conditions. The most extended uninterrupted dry period observed was 80 months since March 1989 in SPI values and 116 months since February 2005 in SPEI values. The lengthiest continuous wet phase recorded was 52 months since April 2009 for SPI values and 51 months since July 1995 for SPEI values. Graphical representations analyzing SPI and SPEI indices before and after the year 2000 are presented in Figure 5.

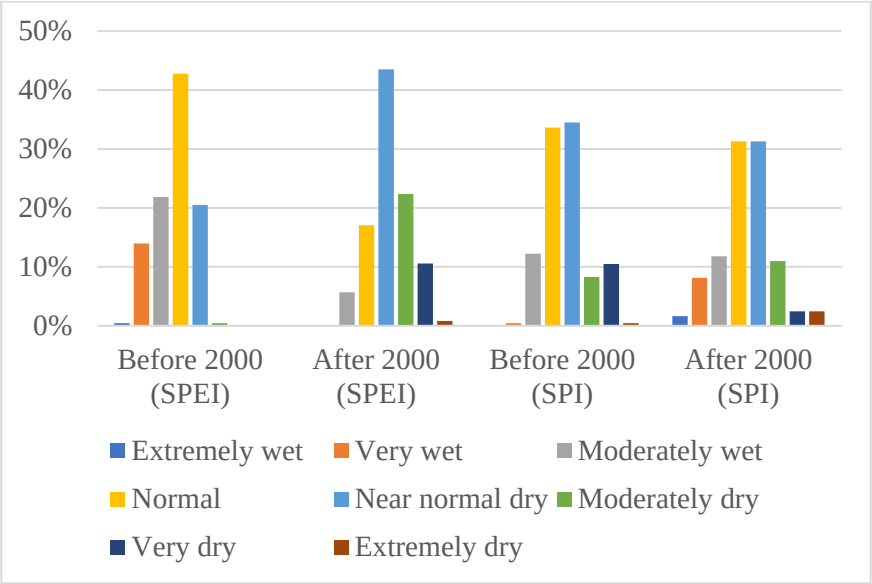

Figure 5: SPI and SPEI values of Konya station before and after 2000

Upon analysis of Figure 5, based on the SPI values, it is apparent that, despite exhibiting continental climate characteristics before the year 2000, the Konya station persisted in a wet period after 2000. Specifically, 130 of the 246 months calculated were categorized as normal and wet. In terms of the SPEI values, a more tranquil distribution was noted before 2000. However, post-2000, there is an observable decrease in the impact of wet conditions and an increase in the severity of dry conditions.

Seydişehir station

The results of SPI and SPEI indices obtained using Seydisehir station data are given in Table 8.

Table 8: Number of drought severity at different time scales at Seydişehir station

Class	Index	1 Month	3 Month	6 Month	12 Month	24 Month
EW	SPI/SPEI	20/11	21/8	18/7	17/5	10/0
VW	SPI/SPEI	18/26	14/29	22/27	29/39	30/36
MW	SPI/SPEI	33/50	36/47	41/57	40/43	54/55
N	SPI/SPEI	150/165	163/176	154/158	140/148	132/145
NND	SPI/SPEI	218/155	185/145	182/160	187/180	174/151
MD	SPI/SPEI	52/63	63/61	52/51	46/34	54/61
VD	SPI/SPEI	7/26	13/27	21/29	27/32	21/26
ED	SPI/SPEI	0/2	1/3	3/4	1/6	0/1

At the Seydişehir station, the analysis of SPI values derived from 12-month data revealed 226 months with wet conditions and 261 months with dry conditions, while corresponding SPEI values indicated 235 months with wet conditions and 252 months with dry conditions. For SPI values calculated over a 24-month period, 226 months were wet, and 249 months were dry, while SPEI values showed 236 months with wet conditions and 239 months with dry conditions. The most extended uninterrupted dry period observed was 63 months since January 1983 in SPI values and 116 months since January 1983 in SPEI values. The lengthiest continuous wet phase recorded was 59 months since February 2009 for SPI values and 58 months since February 2009 for SPEI values. Graphical representations analyzing SPI and SPEI indices before and after the year 2000 are presented in Figure 6.

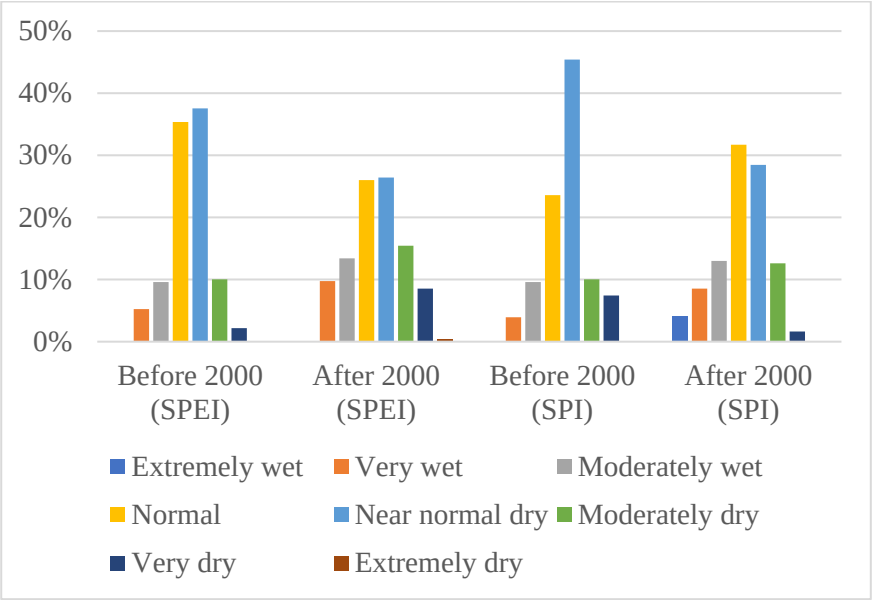

Figure 6: SPI and SPEI values of Seydisehir station before and after 2000

Upon analysis of Figure 10, in accordance with SPI values, it is evident that dry months are more prevalent before the year 2000, whereas wet months are more frequent after 2000. Regarding SPEI values, a more even distribution is observed before 2000, with an escalation in the intensity of both wet and dry conditions noted after 2000.

Conclusion

Drought analysis was conducted in the Ermenek Dam Basin utilizing data obtained from monitoring stations in Alanya, Anamur, Karaman, Konya, and Seydişehir. Despite the evident influence of the Mediterranean climate in the Ermenek district, a basin-oriented perspective reveals transitional characteristics towards a continental climate. In general, both SPI and SPEI values indicate a prevalence

of normal and near-normal drought conditions. Prior to the year 2000, there was a higher occurrence of wet months, contrasting with a notable increase in dry months post-2000. The analysis reveals an augmentation in the values of extremely wet and very wet periods, alongside an increase in extremely dry and very dry conditions. Upon examining the 24-month correlation coefficient between SPI and SPEI indices, stations with high correlation coefficients, such as Anamur (93.5) and Alanya (89.0), where the Mediterranean climate is prominent, are identified. Contrastingly, stations characterized by a continental climate, namely Karaman (66.1), Konya (61.4), and Seydişehir (60.2), exhibit lower correlation coefficients. Upon analysing the correlations between the meteorological stations, it was observed that stations located in areas with Mediterranean climate, such as Alanya and Anamur, had higher correlations among themselves. Conversely, stations located in areas with continental climate, such as Konya, Karaman, and Seydişehir, had higher correlations among themselves. Table 9 presents the correlation values between the stations.

Table 9: Correlation values between the stations

Stations	Alanya	Anamur	Konya	Karaman	Seydişehir
Alanya	1				
Anamur	0.7932	1			
Konya	0.4648	0.4762	1		
Karaman	0.4354	0.5552	0.8476	1	
Seydişehir	0.5414	0.7138	0.7910	0.8174	1

Wet and dry periods manifest at distinct times and with varying intensities among these stations. Notably, the findings suggest that SPEI values offer greater utility compared to SPI values. Considering recent assessments, a discernible trend towards increased dryness in the basin is observed. Consequently, proactive

monitoring of dry periods in the basin is warranted, and the utilization and management of water resources should be adapted accordingly. To combat drought, conserve water resources, and ensure sustainable water management, effective measures must be taken. Campaigns can be organized to promote the efficient use of water, and the adoption of water-saving technologies can be encouraged. Additionally, more efficient irrigation techniques and water loop closure systems should be promoted to reduce water use in agriculture and industrial activities. Water stocks can be created by installing rainwater harvesting systems to collect and store water. Anti-desertification measures, such as preventing soil erosion and carrying out afforestation projects, can also reduce the risk of desertification. These measures can play a crucial role in combating drought, helping to conserve water resources and ensure a sustainable future.

Acknowledgement

This study was produced from the doctoral thesis titled 'Investigation of Climate Change Effects in The Ermenek Dam Basin Using Geographic Information Systems and Remote Sensing Techniques' and is an expanded version of the paper titled 'Drought Analysis Forecast in Ermenek Dam Basin Using SPI and SPEI Indices' presented at the 14th International Conference on Engineering & Natural Sciences. We thank the General Directorate of Meteorology and the State Hydraulic Works for providing data.

References

Akbaş, A. (2014). Türkiye üzerindeki önemli kurak yıllar. *Coğrafi Bilimler Dergisi, 12*(2), 101-118.

Aktürk, G., Zeybekoğlu, U., & Yıldız, O. (2022). SPI ve SPEI yöntemleri ile kuraklık araştırması: Kırıkkale Örneği. *International Journal of Engineering Research and Development, 14*(2), 762-776.

Anisfeld S.C. (2011). *Water resources*. Island Press.

Arslan, O., Bilgil, A., & Veske, O. (2016). Standart yağış indisi yöntemi ile Kızılırmak Havzası'nın meteorolojik kuraklık analizi. *Niğde Ömer Halisdemir Üniversitesi Mühendislik Bilimleri Dergisi, 5*(2), 188-194.

Ashraf, M., & Routray, J. K. (2013). Perception and understanding of drought and coping strategies of farming households in north-west Balochistan. *International Journal of Disaster Risk Reduction*, 5, 49-60.

Bacanlı, Ü. G., & Kargı, P. G. (2019). Uzun ve kısa süreli periyotlarda kuraklık analizi: Bursa örneği. *Doğal Afetler ve Çevre Dergisi, 5*(1), 166-174.

Bae, S., Lee, S. H., Yoo, S. H., & Kim, T. (2018). Analysis of drought intensity and trends using the modified SPEI in South Korea from 1981 to 2010. *Water, 10*(3), 327.

Bakanoğulları, F. (2020). Kırsal havzalarda kuraklığın iki yöntem (SPEI ve SPI) kullanılarak belirlenmesi: Kumdere Havzası örneği. *Türk Tarım ve Doğa Bilimleri Dergisi, 7*(1), 146-156.

Caloiero, T., Veltri, S., Caloiero, P., & Frustaci, F. (2018). Drought analysis in Europe and in the Mediterranean basin using the standardized precipitation index. *Water*, *10*(8), 1043.

Chen, S. T., Kuo, C. C., & Yu, P. S. (2009). Historical trends and variability of meteorological droughts in Taiwan/Tendances historiques et variabilité des sécheresses météorologiques à Taiwan. *Hydrological sciences journal*, *54*(3), 430-441.

Danandeh Mehr, A., & Vaheddoost, B. (2020). Identification of the trends associated with the SPI and SPEI indices across Ankara, Turkey. *Theoretical and Applied Climatology*, *139*(3), 1531-1542.

Erişmiş, M. (2023). Standartlaştırılmış yağış buharlaşma indeksine göre Meriç Nehri Havzasında uzun dönem kuraklık analizi. *International Journal of Geography and Geography Education*, (50), 313-328.

Fontaine, M. M., & Steinemann, A. C. (2009). Assessing vulnerability to natural hazards: impact-based method and application to drought in Washington State. *Natural Hazards Review*, *10*(1), 11-18.

Ilgar, R. (2010). Çanakkale'de kuraklik durumu ve eğilimlerinin standartlaştirilmiş yağiş indisi ile belirlenmesi. *Marmara Coğrafya Dergisi*, (22), 183-204.

Ionita, M., Scholz, P., & Chelcea, S. (2016). Assessment of droughts in Romania using the Standardized Precipitation Index. *Natural Hazards*, 81, 1483-1498.

İrcan, M. R., & Duman, N. (2021). Standartlaştırılmış Yağış İndisi (SYİ) yöntemi ile Şanlıurfa ili kuraklık analizi. *Coğrafya Dergisi*, (42), 1-18.

Kamruzzaman, M., Almazroui, M., Salam, M. A., Mondol, M. A. H., Rahman, M. M., Deb, L., ... & Islam, A. R. M. T. (2022). Spatiotemporal drought analysis in Bangladesh using the standardized precipitation index (SPI) and standardized precipitation evapotranspiration index (SPEI). *Scientific Reports, 12*(1), 20694.

Karaer, M., & Gültaş, H. T. (2018). Kuraklık Oluşumunun Bilecik İli'nde Standartlaştırılmış Yağış İndeksi Yöntemi Kullanılarak Değerlendirilmesi. *Ziraat Fakültesi Dergisi*, 303-308.

Kıymaz, S., Güneş, V., & Asar, M. (2011). Standartlaştırılmış yağış indeksi ile Seyfe Gölünün kuraklık dönemlerinin belirlenmesi. *Journal of Agricultural Faculty of Gaziosmanpaşa University (JAFAG), 2011*(1), 91-102.

McKee, T. B., Doesken, N. J., & Kleist, J. (1993). The relationship of drought frequency and duration to time scales. *In Proceedings of the 8th Conference on Applied Climatology, 17*(22), (pp. 179-183).

Menteşe, S., & Akbulut, S. (2023). Standartlaştırılmış Yağış İndeksi (SYİ) ile Bilecik Merkez İlçe ve Bozüyük İlçesinin Kuraklık Durumunun Belirlenmesi. *Doğu Coğrafya Dergisi, 28*(49), 40-51.

Mishra, A. K., & Singh, V. P. (2011). Drought modeling–A review. *Journal of Hydrology*, *403*(1-2), 157-175.

Pei, Z., Fang, S., Wang, L., & Yang, W. (2020). Comparative analysis of drought indicated by the SPI and SPEI at various timescales in inner Mongolia, China. *Water*, *12*(7), 1925.

Sarış, F., & Gedik, F. (2021). Konya Kapalı Havzası'nda meteorolojik kuraklık analizi. *Coğrafya Dergisi*, (42), 295-308.

Sırdaş, S., & Sen, Z. (2003). Spatio-temporal drought analysis in the Trakya region, Turkey. *Hydrological Sciences Journal, 48*(5), 809-820.

Swed, F. S., & Eisenhart, C. (1943). Tables for testing randomness of grouping in a sequence of alternatives. *The Annals of Mathematical Statistics, 14*(1), 66-87.

Şener, E., & Şener, Ş. (2019). Meteorolojik kuraklığın coğrafi bilgi sistemleri tabanlı zamansal ve konumsal analizi: Çorak Gölü Havzası (Burdur-Türkiye) örneği. *Mühendislik Bilimleri ve Tasarım Dergisi, 7*(3), 596-607.

Şener, E., & Davraz, A. (2021). Yağış tabanlı farklı indisler kullanılarak meteorolojik kuraklık analizi: Isparta örneği. *Mehmet Akif Ersoy Üniversitesi Fen Bilimleri Enstitüsü Dergisi, 12*(Ek Sayı 1), 404-418.

Şener, E., & Şener, Ş. (2021). SPI ve CZI kuraklık indislerinin CBS tabanlı zamansal ve konumsal karşılaştırması: Burdur Gölü Havzası örneği. *Doğal Afetler ve Çevre Dergisi, 7*(1), 41-58.

Taylan, D., & Bahşi, A. M. (2021). Gaziantep ili meteorolojik kuraklık analizi ve KAS ilişkisi. *Süleyman Demirel Üniversitesi Fen Bilimleri Enstitüsü Dergisi, 25*(2), 371-382.

Thornthwaite, C. W. (1948). An approach toward a rational classification of climate. *Geographical review, 38*(1), 55-94.

Tirivarombo, S. O. D. E., Osupile, D., & Eliasson, P. (2018). Drought monitoring and analysis: standardised precipitation evapotranspiration index (SPEI) and standardised precipitation

index (SPI). *Physics and Chemistry of the Earth, Parts A/B/C*, 106, 1-10.

Topçu, E., & Karaçor, F. (2021). Erzurum istasyonunun standartlaştırılmış yağış evapotranspirasyon indeksi ve bütünleşik kuraklık indeksi kullanılarak kuraklık analizi. *Politeknik Dergisi, 24*(2), 565-574.

Uçar, Y., Topçu, E., & Demirel, E. (2019). Standartlaştırılmış Yağış İndeksi Yöntemi ile Isparta İli Kuraklık Analizi. *Türk Bilim ve Mühendislik Dergisi, 1*(1), 5-16.

Vicente-Serrano, S. M., Beguería, S., & López-Moreno, J. I. (2010). A multiscalar drought index sensitive to global warming: the standardized precipitation evapotranspiration index. *Journal of climate, 23*(7), 1696-1718.

Yang, M., Yan, D., Yu, Y., & Yang, Z. (2016). SPEI-based spatiotemporal analysis of drought in Haihe River Basin from 1961 to 2010. *Advances in Meteorology*, 2016, 1-10.

Yetmen, H. (2013). Van Gölü Havzası'nın kuraklık analizi. *21. Yüzyılda Eğitim ve Toplum Eğitim Bilimleri ve Sosyal Araştırmalar Dergisi, 2*(5), 184-198.

Yuce, M. I., & Esit, M. (2021). Drought monitoring in Ceyhan basin, Turkey. *Journal of Applied Water Engineering and Research, 9*(4), 293-314.

Yüce, M. İ., Aksoy, H., Aytek, A., Eşit, M., Uğur, F., Yaşa, İ., Şimşek, A. & Değer, İ. H. (2022). SPI ve SPEI ile Samsun ili kuraklık analizi. *Kahramanmaraş Sütçü İmam Üniversitesi Mühendislik Bilimleri Dergisi, 25*(3), 285-295.

CHAPTER II

Spatial Analysis of Culicoides Biting Midges (Diptera: Ceratopogonidae) in the Western Black Sea Region

Ilkay BUGDAYCI[1]
Melike GOKCE[2]

Introduction

All studies on a particular species in a particular region called faunistic studies. Studies such as the climatic conditions of the region, environmental factors affecting the species, living and breeding conditions are examples of these. As in many areas, Geographic Information System (GIS) is also used for spatial analysis of faunistic researches for living things. GIS provides great advantages in digitizing spatial data of species and processing different attribute information, performing various analyzes and

[1] Necmettin Erbakan University, Department of Geomatics Engineering, Konya,
Orcid: 0000-0001-8361-1306
[2] Cartography Department, General Directrate of Mapping, Ankara
Orcid: 0000-0002-3902-5120

designing species distribution and density maps etc. (Gokce, Bugdayci & Dik, 2019)

GIS is important in faunistic studies especially in terms of creating distribution maps for collection sites of species, determining possible expansion of species, analyzing change and development of faunistic data over time, preventing possible epidemic outbreaks. And it is of great importance when planning vaccinations in regions according to the phenology and ecology of the species that are vectors for diseases, and providing the opportunity for regional intervention in risk areas in case of an epidemic.

Epidemic animal diseases pose a great risk for the environment, human and animal health and national economies. These disease include Bluetongue virus (BTV), Akabane, Bovine Ephemeral Fever (BEF) and Schmallenberg virus (SBV) disease. These infectious diseases are generally transmitted between animals by species of biting midges of the genus *Culicoides*. The most common of these diseases is BTV, and it has caused long-lasting epidemics with great economic losses in many countries over the years (Gorman, Taylor & Walker, 1983; Verwoerd & Erasmus 2004). Due to the devastating effects of this disease, the geographical distribution of the genus *Culicoides*, seasonality breeding sites, environmental factors affecting the species, etc. were determined. GIS is widely used to model the geographical distributions of this genus by associating it with environmental factors, to reveal environmental factors on their distribution, and to predict their distributions in regions that have not been studied before (Rogers & Randolph, 2003). The effect of climate on the emergence and

distribution of *Culicoides* species have been evaluated and modelled (Silbermayr & ark., 2011).

Developments in GIS and spatial modelling methods allow the creation of risk maps for many diseases and the evaluation of vector-borne diseases together with environmental and climatic factors. GIS technologies have become useful tools, especially for ecological analyses, disease mapping, seasonality and surveillance of diseases (Cringoli & ark., 2005). Therefore, GIS technology; are increasingly being used to create risk zones by utilizing environmental and climatic features (Silbermayr & ark., 2011; Blanda & ark., 2018; Goffredo & ark., 2003; Ward & Carpenter, 2000; Conte & ark., 2007; Caligiuri & ark., 2004; Boyer, Ward & Singer, 2010).

In order to follow the spatial and temporal variation of the abundance of the genus *Culicoides* after the BTV epidemic in Europe in 2006, a database study was conducted with the current data of the genus *Culicoides* from Spain, France, Germany, Austria, Switzerland, Denmark, Sweden, Norway and Poland (Cuéllar & ark., 2018). In addition, there are studies where tabular data related to monthly, annual and weekly calculated total abundance of the genus *Culicoides*, maps of study areas, and trap locations are available on the internet (Quaglia & ark., 2020).

In this study, spatial analysis of data available of different *Culicoides* species detected in the Western Black Sea Region of Turkey with meteorological data (humidity, precipitation, temperature, wind) was performed. Density maps of the region designed and the data on species identification presented on Github, which provides free storage for the use of other researchers.

Obtaining, storing and accessing information about location, population, distribution, disease, etc. about *Culicoides* and other species will aid other researchers in their studies.

Culicoides

Culicoides species belong to the suborder Nematocera, and family Ceratopogonidae. To date, approximately 1400 *Culicoides* species have been described World wide world (Borkent, 2021), of which 61 have also been found in Turkey (Dik, 2017). The females of these flies, are 1-3 mm in size, feed on blood from humans and animals, and the males feed on plant sap (Blackwell, 2001). They are vectors for diseases such as BTV, Akabane, BEF and SBV. These viruses may cause miscarriage in pregnant animals, hydrocephalus, microcephaly and other disorders related to the nervous system of newborn calves, lambs and kids, infertility, decrease in meat and milk production and may result in the death of adult animals. In humans and especially equine (horses, donkeys, etc.), they may cause various skin reactions such as temporary burning, mild swelling and itching in the places where they suck blood, and may cause blistering and allergic reactions in more sensitive individuals.

The widespread spread outbreaks of BTV in Europe and the recent emergence of Schmallenberg's disease have raised concerns that the African horse sickness virus may also spread to temperate regions of the world (Sanchez-Matamoros & ark., 2016). *Culicoides* monitoring have intensified since the emergence of SBV as well as BTV (Leta & ark., 2019).

According to Baylis et al. (Baylis & ark., 2017), BTV disease was first discovered in South Africa in the early 20th century and was considered an African disease until another outbreak occurred

in Cyprus in 1943 (Mellor, Baylis & Mertens, 2009. Later, two more outbreaks occurred in Europe. The first was in southern Iberia (1956-1960), which included Spain and Portugal, and the second was on the Greek islands between 1979 and 1980 (Lesbos and Rhodes). It continued with other outbreaks in the Middle East. Shortly after, the virus was found to be present in North America, then also in South Asia and Australia (Baylis & ark., 2017).

BTV re-emerged on the Greek islands in 1998. This time, however, the outbreak was the beginning of the largest BTV outbreak ever seen (Baylis & ark., 2017). The disease affected numerous countries, including those not affected by previous outbreaks, and persisted in some for up to 4 years (Mellor & Wittmann, 2002). This disease, which was previously thought to be limited to regions between latitudes 35° South and 40° North (Gómez, 2004), suddenly appeared in 2006, especially in Belgium, Germany and the Netherlands (Bluetongue in the Netherlands, 2021; Bluetongue in Belgium, 2021; Bluetongue in Germany, 2021). Since then, it has also spread to these countries and neighboring countries (Carpenter et al., 2009). The 1998 outbreak was associated with C. imicola, and the 2006 outbreak in northern and western Europe was associated with C. obsoletus and C. pulicaris (Leta & ark., 2019).

Cyanosis occurs in the mouth lesions of heavily infected animals and dark blue tongue appearance is the characteristic finding of the disease (Saltik & Kale, 2017). BTV has spread to many geographies in the world and can be seen in Turkey from time to time depending on seasonal factors. In addition to causing a large amount of economic losses in Turkey and the world, this virus also causes various health problems in domestic ruminants (Dik, Yagci

& Linton, 2006). Therefore, determining the regions where Culicoides species are found, drying the breeding areas such as swamps and ponds close to these regions, determining the susceptible animal populations in these regions, applying vaccines, and carrying out protection and control studies will be effective methods in epidemic (Saltik & Kale, 2017).

Many variables affect the emergence of *Culicoides* species. Species are spatially separated based on habitat, breeding and feeding requirements. For all analyzed species, various land cover variables and climatic variables affect their emergence positively or negatively in different seasons. For example; *C. imicola* species are mostly affected positively by agricultural areas (fruit trees and fruit fields), while species in *C. pulicaris* and *C. obsoletus* groups are negatively affected by agricultural and forestry areas. *C. newsteadi* species is attached to water fields (natural or artificial drainage channels with a width of at least 100 m) as well as agricultural areas. Climatic variables also affect the formation of Culicoides species. For example, *C. imicola* and *C. newsteadi* species depend on high average temperatures. Species in the *C. pulicaris* and *C. obsoletus* groups are particularly affected by low average temperatures during the wettest quarter of the year (autumn, spring and winter) (Ramilo & ark., 2017). In order to determine the seasonal variables affecting the *Culicoides* species, many studies consisting of long-term observations from different locations have been conducted. For example, in a study conducted in Austria, weekly data were collected for 14 months from 54 capture sites. It was determined that the weather data, average temperature, wind, relative humidity and altitude in these regions were the determining factors on *Culicoides* species. As a result of the study, it has been determined that most of

the capture environments are above 10°C and relative humidity between 60-80% and generally at an altitude below 1300 m (Silbermayr & ark., 2011; Gokce, 2021).

Temperature is critical for the life cycle of *Culicoides* and for the development of the bluetongue virus in the bodies of adult flies. However, the emergence of bluetongue is not only dependent on temperature. In addition to temperature, some factors must also be present in order for *Culicoides* species to reach sufficient maturity and perform their flight activities. These are light, wind, humidity, rain and altitude.

In some studies, it has been stated that the most suitable temperature for the flight activities of *Culicoides* is 13–24 °C. In addition, it has been determined that they do not fly in an environment with little or no wind and at temperatures below 9–10 °C (Dzhafarov, 1976; Blackwell & ark., 1992; Dik, 2017). It was determined that the number of *Culicoides* captured decreased on days when the air temperature was below 15 °C, and increased on days when the temperature was 20 °C and above (Dik, Yagci & Linton, 2006). Adults of *Culicoides* tend to be active during the coldest months, when the mean daily maximum temperature is higher than 12.5 °C (Sellers & Mellor, 1993; Mellor, Boorman & Baylis, 2000).

Wind is another critical factor for *Culicoides*. It was stated that *Culicoides* fly in windless weather or in weather where the wind speed is less than 2 m/s (Dik, 2017; Elbers, Koenraadt & Meiswinkel, 2015). When the long-range flying potential of some *Culicoides* species is evaluated, the wind-assisted flight motion recorded over hundreds of kilometers is of great interest (Burgin &

ark., 2013; Eagles & ark., 2014; Kelso & Milne, 2014). Studies on long-range flight can help determine risky periods when *Culicoides* carrying viruses can travel long distances with the help of wind (Mullens & ark., 2015). When the paths followed by the winds and the countries where the bluetongue outbreaks are examined, it is stated that the diseases carried by *Culicoides* spread in a short time with the effect of the wind, and they are carried to overseas distances and cause the infection (Duncheyne & ark., 2007).

One of the factors that have a positive effect on the flight of *Culicoides* is humidity (Dik, 2017; Dipeolu & Ogunrinade, 1977; Walker, 1977). It has been noted that when the humidity is reduced to 50%, the flight movements' decrease, and between 60-95% it does not affect the flight movements (Dzhafarov, 1976; Parker, 1949).

Light rain does not affect the flight movements of the *Culicoides* species (Dik, 2017; Dzhafarov, 1976; Walker, 1977; Parker, 1949). In heavy rain, the flight movements of *Culicoides* stop completely (Dzhafarov, 1976; Dipeolu & Ogunrinade, 1977; Sellers & Pedgley, 1979). However, *Culicoides* continue their flight activities indoors in rainy weather (Dik, 2017).

Culicoides species can survive at different altitudes. Since *C. imicola* is considered the main bluetongue vector in Europe, the places where the probability of catching *C. imicola* is highest were chosen as trap sites first, based on published information on temperature, altitude, and host requirements. *C. imicola* appears to be most common at altitudes below 260 m, although it sometimes reaches up to 460 m (Torina & ark., 2004). However, the distribution of *C. obsoletus* complex and *C. pulicaris* complex can also be seen at higher altitudes. Most of the *C. obsoletus* complex abundance has

been recorded at areas lower than 1109 m. He defined it as the highest place of *C. obsoletus* complex formation in Italy at an altitude of 1211 m (Torina & ark., 2004).

Materials and Methods

GIS supports the users in the decision-making process with the help of spatial analysis. Regardless of the area where the spatial analysis studies are carried out, during the creation of the maps; GIS is used in processes such as collecting, processing and storing data. In this study, the data on the *Culicoides* species of the study by Dik et al. (Dik & Kuclu, 2017) in the Western Black Sea region was used. *Culicoides obsoletus, C. picturatus, C.punctatus, C. pulicaris* and *C. subfascipennis* were determined to be the dominant species in the same location. The Power BI program is often used for spatial graphing, analysis, and reporting, was used in the production of graphic data of dominant species, and ArcGIS software was used to show the capture locations on the map. ArcGIS works on a database basis and has wide use in many areas because it provides solutions to location-based analysis problems used for the management, design and planning of geographic information (Law & Collins, 2013).

Meteorological parameters such as temperature, precipitation, wind and humidity were obtained meteorological stations. Spatial distributions of these types of data used in many studies (hydrology, agriculture, ecology etc. studies). GIS software provides convenience in obtaining the areal distributions of point climate data. Temperature, precipitation, wind and humidity data were used which were measured hourly from the stations in the Western Black Sea region and obtained from the General Directorate

of Meteorology (GDM). Figure 1 shows the distribution of station points and study area. Analysis were carried out to establish the quarterly (June, July, August) average data based on the hourly data between 20-24 hours (the capture hours) and the location of the station data from the GDM were correlated with the average data from the meteorological data.

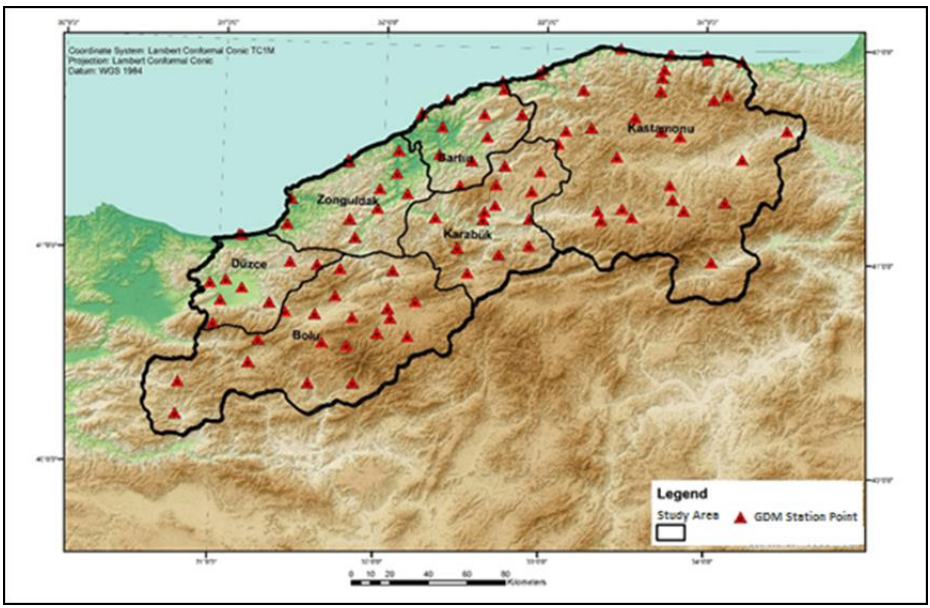

Figure 1: The Station Points of General Directorate of Meteorology (GDM) and Study Area

Thematic maps were designed for each meteorological data with the IDW interpolation method from the meteorological data (temperature, precipitation, humidity and wind) provided by GDM, which is considered to be important for reproduction, life and flight activities of *Culicoides* species. Spatial analysis studies were carried out by superimposing the *Culicoides* data onto the maps. The Mean Square Error (MSE) was used for the accuracy criterion of these

maps. For accuracy analysis, some of the meteorological stations were reserved for verification and the interpolation process for each meteorological data was applied without this data. Taking into account the difference between the real values obtained from the GDM of the control stations and the calculated surface values, MSE was calculated for each meteorological data, and the accuracy of the method was checked. The MSE calculated as follows (Equation);

$$MSE = \pm\sqrt{((\sum_{i=1}^{n} [\![\varepsilon_i^2]\!])/n)} = \pm\sqrt{(([\varepsilon\varepsilon])/n)} \quad (1)$$

ε_i=Error (observed values-predicted values)

n = number of data points

Results and Discussion

Within the samples collected during the study by Dik & et al (2017) *C. obsoletus, C. picturatus, C.punctatus, C. pulicaris and C. subfascipennis*, were the dominant species collected (Figure 2). Figure 3 shows the data on the numbers of *Culicoides* species caught in the Western Black Sea Region.

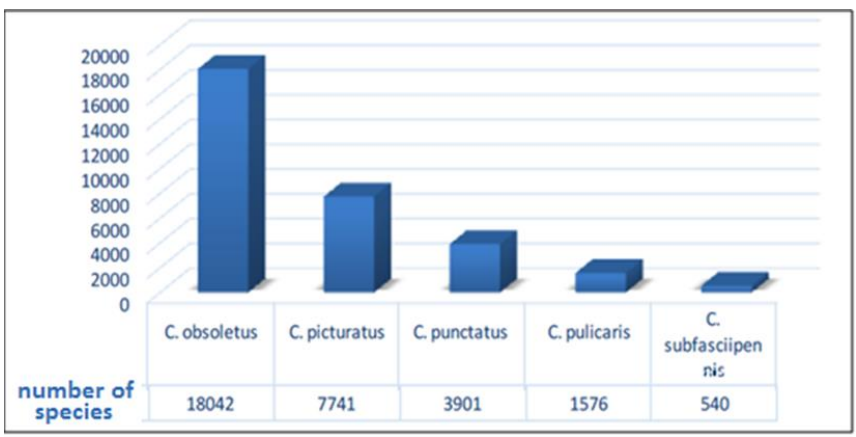

Figure 2: Dominant Species of the Western Black Sea Region (Dik & Kuçlu, 2017)

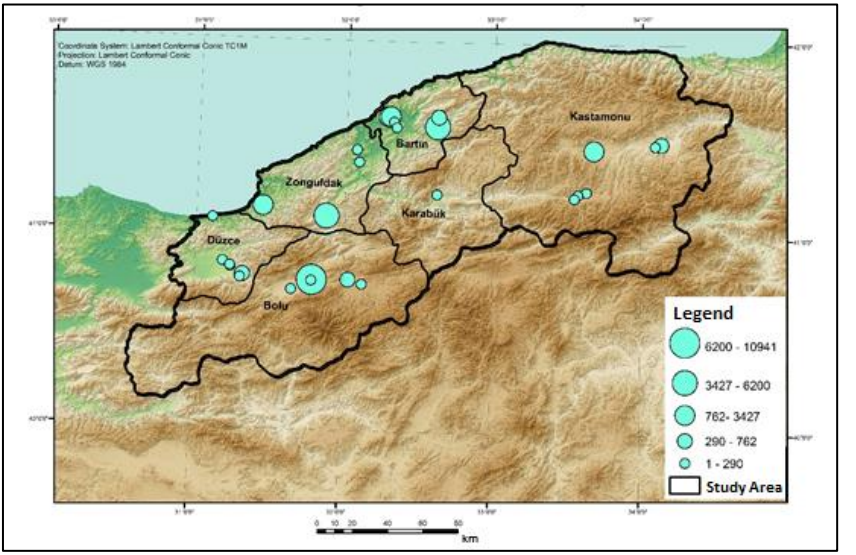

Figure 3: Data on the numbers of Culicoides caught in the Western Black Sea Region

The total of dominant species at the collection points were transformed into spatial graphic data with the PowerBI program in order to show the percentage of dominant species among the collected samples. The collection point of the 5 dominant species within the species is indicated, and the analysis data regarding the number and percentage of the detected species are presented spatially.

Maps were designed for each of meteorological parameters, taking into account the climate data required for breeding and flight activities of *Culicoides* species. Spatial analysis was carried out to determine the suitability of living and breeding conditions of each regions.

Temperature is an important factor in the life cycle and flight activities of *Culicoides*. For the realization of flight activities, the

most suitable temperature should be between 13-24 °C. Analysis of the temperature map (Figure 4), that the region has a suitable temperature for the survival of *Culicoides* species in general.

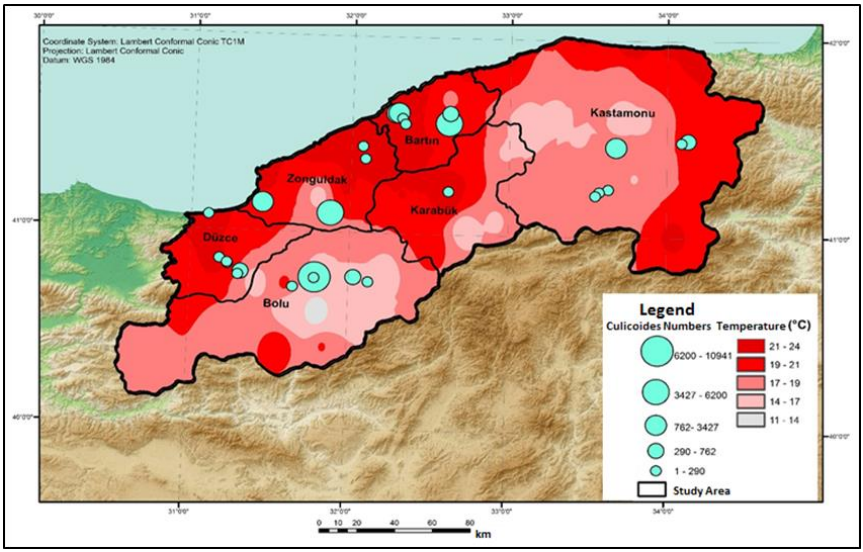

Figure 4: Temperature map of Western Black Sea Region

In the species identification study carried out in the Western Black Sea region, the captured areas of *Culicoides* species are usually sheep and cattle pens or chicken or poultry and turkey pens, and flight activities of *Culicoides* species continue as these areas are not affected by the wind. For the flight of *Culicoides* species, the optimum wind speed should be 2 mm/sec or less. Evaluation of the map for the wind (Figure 5) and the number of *Culicoides* captured in the region indicate that more *Culicoides* are caught in regions where the wind speed is lower than 2 mm/s.

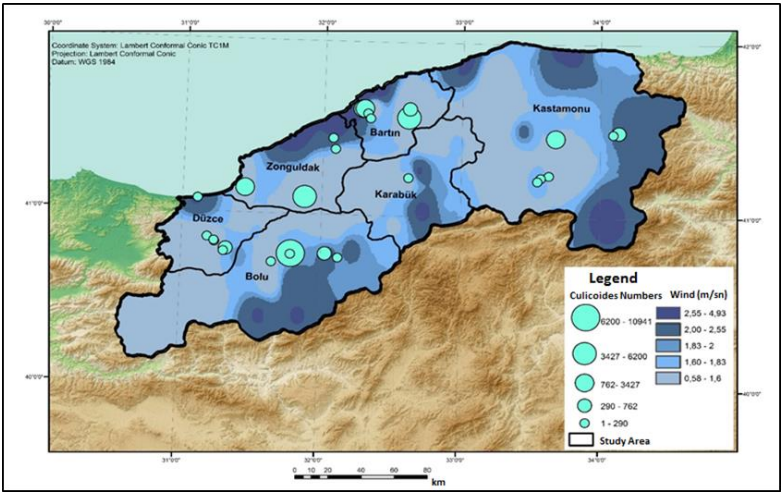

Figure 5: Wind map of Western Black Sea Region

Humidity is another important factor for flight activity. Flight decrease when humidity is reduced to 50%, but has no affect between 60-95%. The humidity map (Figure 6) indicates that the *Culicoides* numbers are higher in regions where the humidity is between 65-99%.

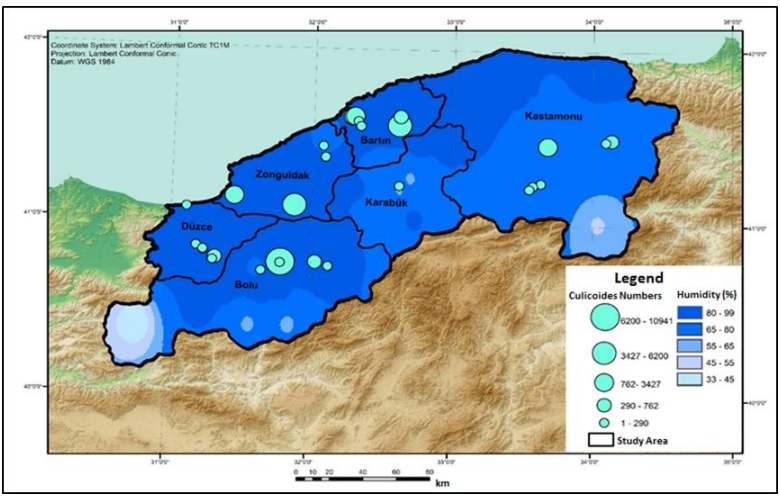

Figure 6: Humidty map of Western Black Sea Region

Culicoides flight activities continue indoors in rainy weather with light precipitation but stops in heavy rains. Since most of the summer months of 2014 were without precipitation and *Culicoides* were caught in the pens, it is thought that precipitation did not have a great effect on the number of seizures. However, when the precipitation map (Figure 7) and the number of *Culicoides* captures are compared, it is seen that the numbers overlap in general.

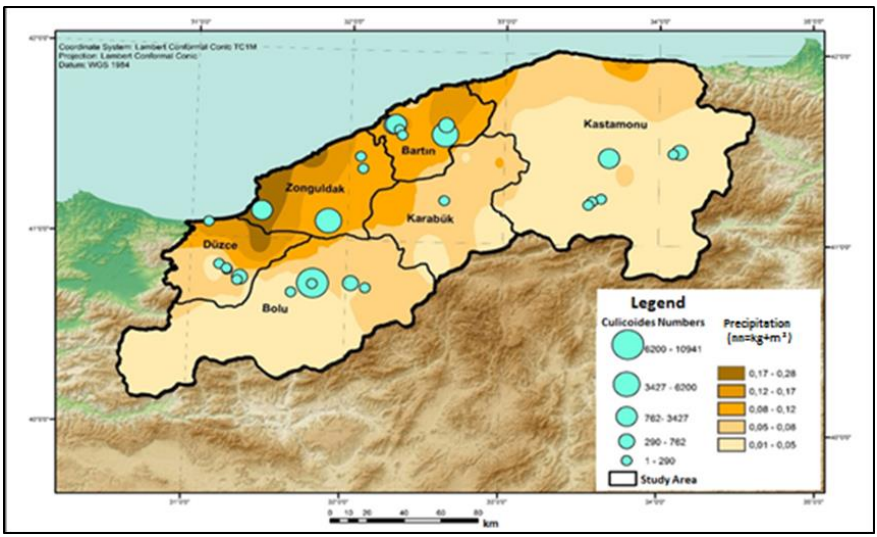

Figure 7: Precipitation map of Western Black Sea Region

The MSE calculations for meteorological data are given in Tables 1-4. The accuracy analysis of the method used was made with MSE. Considering the MSE values; 1.29 (°C) for temperature data (Table 1.), 1.48(m/s) for wind data (Table 2), 8.61(%) for humidity data (Table 3) and 0.05(mm=kg÷m²) for precipitation data (Table 4). The lowest MSE value was calculated for precipitation. The IDW method gives the best results for precipitation from meteorological data. The MSE value calculated for humidity is high, leading us to conclude that the IDW method used for interpolation of moisture

data is not very suitable. However, when the map created with the humidity data (Figure 6) and the *Culicoides* numbers detected in the region are examined together, it is seen that the number of *Culicoides* is higher in the regions where the humidity is between 65-99% on the map, and the map generally overlaps with the *Culicoides* numbers. For this reason, a different interpolation process was not applied for moisture data. It is considered that it would be more appropriate to conduct a different study comparing interpolation techniques for moisture data.

Table 1: The MSE calculation of temperature data

Station Number	Latitude	Longitude	Calculated Surface Value	GDM Value	Error	Error square
17615	41,55589	32,67176	20,65694	20,066774	0,590166	0,34829591
17721	41,6872	32,6156	21,08532	18,287826	2,797494	7,82597268
18260	40,9725	31,44	19,287128	19,102011	0,185117	0,0342683
18262	41,1983	32,3267	20,566347	21,022733	-0,456386	0,20828818
18515	41,5	33,4439	17,16883	16,931379	0,237451	0,05638298
18522	41,4942	34,2225	19,20743	20,458333	-1,250903	1,56475832
						∑ =10,037966
						MSE=1,293442

Table 2: The MSE calculation of wind data

Station Number	Latitude	Longitude	Calculated Surface Value	GDM Value	Error	Error square
17615	41,55589	32,67176	0,075096	0,745714	-0,67061829	0,44972889
17721	41,6872	32,6156	0,096582	0,8	-0,703418	0,49479688
18260	40,9725	31,44	0,110291	1,504961	-1,39467069	1,94510632
18262	41,1983	32,3267	0,07131	0,977616	-0,90630628	0,82139107
18515	41,5	33,4439	0,04015	2,135689	-2,09553966	4,39128645
18522	41,4942	34,2225	0,051763	2,287528	-2,23576574	4,99864842
						∑ =13,100958
						MSE=1,4776647

Table 3: The MSE calculation of humidity data

Station Number	Latitude	Longitude	Calculated Surface Value	GDM Value	Error	Error square
17615	41,55589	32,6717	79,713905	90,29596774	-10,5820627	111,980052
17721	41,6872	32,6156	80,801979	91,73695652	-10,9349775	119,573733
18260	40,9725	31,44	88,361626	86,45517241	1,906453586	3,63456528
18262	41,1983	32,3267	77,541161	81,27267442	-3,73151342	13,9241924
18515	41,5	33,4439	77,262764	73,23103448	4,031729517	16,2548429
18522	41,4942	34,2225	78,734802	65,32988506	13,40491694	179,691798
						∑ =445,05918
						MSE=8,61257

Table 4: The MSE calculation of precipitation data

Station Number	Latitude	Longitude	Calculated Surface Value	GDM Value	Error	Error square
17615	41,55589	32,67176	0,075096	0,119036	-0,04394	0,00193072
17721	41,6872	32,6156	0,096582	0,170435	-0,073853	0,00545427
18260	40,9725	31,44	0,110291	0,197241	-0,08695	0,0075603
18262	41,1983	32,3267	0,07131	0,09907	-0,02776	0,00077062
18515	41,5	33,4439	0,04004	0,01839	0,02165	0,00046872
18522	41,4942	34,2225	0,051763	0,01908	0,032683	0,00106818
						∑ =0,01725281
						MSE=0,05362339

Conclusions

Some *Culicoides* biting midges play an active role as vectors in the spread of diseases such as BTV and SBV. For example, *C. imicola* was considered to be the main vector of BTV, but it was found that *C. obsoletus and C.pulicaris* were the vectors in the outbreaks in Europe in the areas where C. imicola were rare. *Culicoides obsoletus* and C. pulicaris groups have been shown as the main vectors for SBV, a recently emerged and are still spreading disease. For this purpose, further analysis of the data collected by Dik et al. [45] during their study in the Western Black Sea region was done. Number of collections for *C. obsoletus, C.picturatus, C. punctatus, C. pulicaris and C. subfascipennis* per collection site and their percentage among other species are shown as location-based graphic data. The Power BI program was used for producing graphic data of dominant species; ArcGIS program was used to design the maps. Meteorological data obtained from the GDM of the study area, maps designed according to the values obtained by using the IDW method, for the interpolation of this data.

The accuracy analysis of the method used was made with MSE. Considering the MSE values; 1.29 (°C) for temperature data (Table 1.), 1.48(m/s) for wind data (Table 2), 8.61(%) for humidity data (Table 3) and 0.05(mm=kg÷m²) for precipitation data (Table 4).

The temperature must be between 13-24 °C in order to perform the flight activities of *Culicoides* (Figure 4). For the flight of *Culicoides* species, the optimum wind speed should be 2 mm/sec or less. With the map created for the wind (Figure 5), it was seen that *Culicoides* were caught more in the regions where the wind speed is 2 mm/sec and less. The number of *Culicoides* is higher in the regions where the humidity is between 65-99% on the map (Figure 6). While the flight activities of *Culicoides* are not affected in light rainy weather, it stops in heavy rains. Precipitation is not thought to have a major impact, as *Culicoides* are usually caught in the sheep or cattle pens or chicken and turkey pens. However, when the precipitation map (Figure 7) and the number of *Culicoides* captures are compared, it is seen that the numbers overlap in general.

In order to better analyze the spatial distribution and distribution of the species belonging to the genus *Culicoides*, besides meteorological data; It was concluded that it would be more appropriate to conduct a comprehensive study based on long-term observation data by including other data such as vegetation cover, susceptible animal population, soil structure of the land.

It is important to record and store data such as species identification and follow-up studies of the distribution of the species, animal populations in study areas, the identification of susceptible host species, detection of antibodies and even the number of species described in a database. There is no such study yet for the *Culicoides* species in Turkey. For this reason, in this study, the aim was to provide quick and easy access regarding information about the species determination for veterinarians, other researchers who are interested in this genus. In this context, the species identification

study used in this paper was recorded. Data such as the location (latitude, longitude, and altitude), capture conditions (weather, temperature, and inside/outside of the barns or pens), number of traps, date of capture, species information detected are tabulated and presented freely on Github (https://melikegokce.github.io/tez/).

Acknowledgments: The authors would like to thank, Bilal DIK, Ozge KUCLU, Rahile OZTURK for the contribution of the project namely "*Culicoides* Latreille, 1809 (Diptera: Ceratopogonidae) species in the Western Black Sea Region of Turkey, new records for the Turkish fauna *Culicoides* data of Turkish fauna in Western Black Sea Region of Turkey". This study was produced from Melike Gokce's master thesis completed at Necmettin Erbakan University, Institute of Science and Technology. This study was produced from Melike Gokce's master thesis completed at Necmettin Erbakan University, Institute of Science and Technology.

References

Baylis, M., Caminade, C., Turner, J., & Jones, A.E. (2017). The role of climate change in a developing threat: the case of bluetongue in Europe. *Rev. Sci. Tech. Off. Int. Epiz, 36, 2*, 467-478.

Blackwell, A. (2001). Recent advances on the ecology and behaviour of Culicoides spp.in Scotland and the prospects for control. *Vet. Bull. 71, 11*, 1-8.

Blackwell, A., Mordue, A.J., Young, M. R., & Mordue, W. Bivoltinism. (1992). Survival rates and reproductive characteristics of the Scottish bitingmidge, Culicoides impunctatus (Diptera: Ceratopogonidae) inScotland. *Bull. Entomol. Res.*82, 299–306.

Blanda, V. Blanda, M. La Russa, F. Scimeca, R. Scimeca, S. D'Agostino, R. Auteri, M., & Torina, A. (2018). Geo-statistical analysis of Culicoides spp. distribution and abundance in Sicily, Italy. *Parasit. Vectors, 11, 78*

Bluetongue in Belgium. OIE Disease, Information 34: 616. Available online: http://www.oie.int/eng/info/hebdo/AIS_02.HTM (accessed on 15 July 2021)

Bluetongue in Germany. OIE Disease, Information 34: 618. Available online : http://www.oie.int/eng/info/ hebdo/AIS_04.HTM (accessed on 15 July 2021)

Bluetongue in the Netherlands. OIE, Disease Information 34: 612. Available online: http://www.oie.int/eng/info/hebdo/AIS_03.HTM (accessed on 15 July 2021)

Borkent, A. World species of biting midges (Diptera: Ceratopogonidae). Available online: http://wwx.inhs.illinois.edu/files/4514/6410/0252/CeratopogonidaeCatalog.pdf (accessed on 18 June 2021).

Boyer, T.C. Ward, M.P., & Singer, R.S., (2010). Climate, Landscape, and the Risk of Orbivirus Exposure in Cattle in Illinois and Western Indiana. *Am. J. Trop. Med. Hyg. 83,* 789-794.

Burgin, L.E., Gloster, J., Sanders, C., Mellor, P.S., Gubbins, S., & Carpenter, S. (2013). Investigating incursions of bluetongue virus using a model of long-distance Culicoides biting midge dispersal. *Transbound Emerg Dis, 60,* 263-272.

Caligiuri V., Giuliano G.A., Vitale V., Chiavacci L., Travaglio S., Manelli L., Piscedda S., Giardina M., & Mainolfi R., (2004). Bluetongue surveillance in the Campania Region of Italy using a geographic information system to create risk maps. *Vet. Ital. 40, 3,* 385-389.

Conte, A., Goffredo, M., Ippoliti, C., Meiswinkel, R. (2007). Influence of biotic and abiotic factors on the distribution and abundance of Culicoides imicola and the Obsoletus complex in Italy. *Vet Parasitol. 150,* 333–344.

Cringoli, G., Rinaldi, L., Veneziano, V., & Musella, V., (2005). Disease mapping and risk assessment in veterinary parasitology: some case studies. *Parassitologia, 47,* 9–25.

Cuéllar, A.C., Kjær, L.J., Kirkeby, C., Skovgard, H., Nielsen, S.A., & Stockmarr, A., (2018). Spatial and temporal variation in the abundance of Culicoides biting midges (Diptera: Ceratopogonidae) in nine European countries. *Parasites & Vectors. 11,* 112.

Dik, B., (2017). Culicoides'ler (Dıptera: Ceratopogonıdae), Vectors and challenge. 20th National Congress On Parasitology with International Participation, Eskisehir, Turkey, 25-29 September.

Dik, B., Kuclu, O., & Oztürk, R., (2017). *Culicoides* Latreille, 1809 (Diptera: Ceratopogonidae) species in the Western Black Sea Region of Turkey, new records for the Turkish fauna. *Turkish J. Vet. Anim. Sci. 41*, 228-237.

Dik, B., Yagci, Ş., & Linton, Y.M., (2006). A review of species diversity and distribution of Culicoides Latreille, 1809 (Diptera: Ceratopogonidae) in Turkey. *J Nat Hist, 40*, 1947–1967.

Dipeolu, O.O., & Ogunrinade, A.F., (1977). Studies on *Culicoides* species of Nigeria. VII. The biology of some Nigerian *Culicoides* species. *Z Parasitkde, 51*, 289–298.

Duncheyne, E., De Dekens, R., Becu, S., Codina, B., Nomikou, K., Mangana-Vougiaki O., Georgiev, G., Purse, B.V., & Hendickx, G. (2007). Qualifying the wind dispersal of culicoides species in Greece and Bulgaria. *Geospat Health, 1, 2*, 177-189.

Dzhafarov, S.M., (1976). Biting midges (Diptera: Heleidae) of Transcaucasus (morphology, biology, ecology, geographical distribution and harmfulness, control. Fauna of the genera Culicoides, Leptoconops and Lasiohelea). Franklin Book Programs: Cairo.

Eagles, D., Melville, L., Weir, R., Davis, S., Bellis, G., Zalucki, M.P., Walker, P.J., & Durr, P.A., (2014). Long-distance aerial dispersal modeling of Culicoides biting midges: case studies of incursions into Australia. *BMC Vet Re*s, *10*, 135.

Elbers, A.R.W., Koenraadt, C.J.M., Meiswinkel, R., (2015). Mosquitoes and Culicoides biting midges: vector range and influence of climate change. *Rev Sci Tech Off Int Epiz***,** *34*, 123-137.

Goffredo, M., Conte, A., Cocciolito, R., & Meiswinkel, R. Distribuzione (2003). Abbondanza di *Culicoides* imicola in Italia. *Vet. Ital., 47*, 22-32.

Gokce, M., (2021). Construction of Density Map And Spatial Analysis of Culicoides (Diptera: Ceratopogonidae) Flies In The Western Black Sea Region. Master Thesis, Necmettin Erbakan University, Konya, Turkey.

Gokce, M., Bugdayci, I., & Dik B., (2019). The usage of Geographıcal Informatıon System in faunustic research. 7th International Symposium on Academic Studies in Science, Engineering and Architecture, Ankara, Turkey, 15-17 November.

Gómez-Tejedor, C., (2004). Global situation. Brief overview of the bluetongue situation in Mediterranean Europe 1998–2004. Vet. Ital., 40, 57–60.

Gorman, B. M., Taylor, J., & Walker, R.J., (1983). *Orbiviruses*; The Reoviridae; New York, London, pp.287–357.

Kelso, J.K., & Milne, G.J., (2014). A spatial simulation model for the dispersal of the bluetongue vector Culicoides brevitarsis in Australia. *PLoS ONE*, 9.

Law, M., & Collins A., (2013). *Getting to know ArcGIS for desktop*, 4th ed; ESRI press: Canada.

Leta, S., Fetene, E., Mulatu, T., Amenu, K., Jaleta, M.B., Beyene, T.J., Negussie, H., & Kriticos, D., (2019). Updating the

global occurrence of Culicoides imicola, a vector for emerging viral diseases. *Sci. Data*, *6*,185.

Mellor, P., Baylis, M., & Mertens, P.P.C., (2009). *Introduction In Bluetongue*. Academic Press: Amsterdam; pp. 1–6.

Mellor, P.S., Boorman, J., & Baylis, M., (2000). Culicoides biting midges: their role as arbovirus vectors. *Annu. Rev. Entomol*. 45, 307–340.

Mellor, P.S., & Wittmann, E.J., (2002). Bluetongue virus in the Mediterranean Basin 1998-2001. *Vet. J., 164*, 20-37.

Mullens, B., Duranti, A., McDertmott, E.G., & Gerry, A.C., (2015). Progress and knowledge gaps in Culicoides ecology and control. *Vet. Ital. 51*, 313–323.

Parker, A.H., (1949). Observations on the seasonal and daily incidence of certain biting midges (*Culicoides* Latreille-Diptera, Ceratopogonidae) in Scotland. *Trans R Ent Soc Lond***,** *100*, 179–190.

Quaglia, A.I., Blosser, E. M., McGregor, B.L., Runkel, A.E., Sloyer, K.E., Erram, D., &nWisely, S.M., (2020). Burkett-Cadena ND. Tracking Community Timing: Pattern and Determinants of Seasonality in Culicoides (Diptera: Ceratopogonidae) in Northern Florida. *Viruses*, *12*, 931.

Ramilo, D. W., Nunes, T., Madeira, S., Boinas, F., Fonseca, I., (2017). P. Geographical distribution of Culicoides (Diptera: Ceratopogonidae) in mainland Portugal: Presence/absence modelling of vector and potential vector species. *PLoS ONE*, *12*, 7.

Rogers, D.J., & Randolph, S.E., (2003). Studying the global distribution of infectious diseases using GIS and RS; *Nat Rev Microbiol***,** 231– 236.

Saltik, H. S., & Kale, M., (2017). Bluetongue Virus Disease. *MAKU J. Health Sci. Inst., 5, 1,* 32-44.

Sanchez-Matamoros. A., Sanchez-Vizcaino. J. M., Rodriguez-Prieto, V., Iglesias, E., & Martinez-Lopez, B., (2016). Identification of Suitable Areas for African Horse Sickness Virus Infections in Spanish Equine Populations. *Transbound. Emerg. Dis., 63,* 564–573.

Sellers, R. F., & Mellor, P.S., (1993). Temperature and the persistence of viruses in Culicoides spp. during adverse conditions. *Rev Sci Tech Off Int Epiz, 12,* 733 – 755 .

Sellers, R.F., & Pedgley, D.E., (1979). Possible windborne spread to Western Turkey of bluetongue virus in 1977 and of akabane virus in 1979. *J Hyg Camb, 19859, 5,* 149–158.

Silbermayr, K., Hackländer, K., Doscher, C., Koefer, J., & Fuchs, K. A., (2011). Spatial assessment of *Culicoides* spp. distribution and bluetongue disease risk areas in Austria. *Berl. Munch. Tierarztl. Wochenschr, 5-6,* 222–235.

Torina A., Caracappa, S., Mellor, P. S., Baylis M., & Purse, B. V., (2004). Spatial distribution of bluetongue virus and its *Culicoides* vectors in Sicily . *Med. Vet. Entomol, 18,* 81–89.

Verwoerd, D., & Erasmus, B.J., (2004). *Bluetongue, Infectious Diseases of Livestock*; JA Coetzer and RC Tustin; Oxford University Press, Cape Town; pp.1201–1220.

Walker, A.R., (1977). Seasonal fluctuations of *Culicoides* species (Diptera: Ceratopogonidae) in Kenya. *Bull ent Res*, *67*, 217–233.

Ward, M.P., (2000). Carpenter, T.E. Techniques for analysis of disease clustering in space and in time in veterinary epidemiology. *Rev. Prev. Vet. Med*., *45*, 257-284.

CHAPTER III

Trend Analysis of Temperature and Precipitation in Ermenek Dam Basin

Süleyman Savaş DURDURAN[1]
Cafer Tayyar OKKA [2]
Tansu ALKAN[3,4]

Introduction

The developing world, escalating human demands, and rapid technological advancements contribute to the emission of greenhouse gases into the atmosphere. This phenomenon leads to rising temperatures, glacier melting, and the observation of global climate change (Oğuz & Oğuz, 2020). Climate change is a complex occurrence influenced by both human-induced factors and natural

[1] Necmettin Erbakan University, Department of Geomatics Engineering, Konya, Orcid: 0000-0003-0509-4037
[2] State Hydraulic Works 4th Regional Directorate, Konya, Orcid: 0000-0001-8338-8431
[3] Niğde Ömer Halisdemir University, Department of Geomatics Engineering, Niğde, Orcid: 0000-0001-8293-2765
[4] Necmettin Erbakan University, Institute of Science, Konya

events. In recent times, there has been a notable surge in extreme weather events linked to climate change.

The analysis of climatic changes necessitates the use of meteorological parameters such as temperature, precipitation, humidity, wind, and pressure over extended periods. Temperature and precipitation, particularly, are fundamental climate parameters. The fifth assessment report of the Intergovernmental Panel on Climate Change underscores significant alterations in temperature and precipitation values observed across various global regions (Kankal & Akçay, 2019). The subsequent sixth report asserts that climate change is accelerating, attributing human-induced impacts to extreme weather events on a global scale, thereby affecting the world's climate system (Karakuş & Güler, 2022).

Given the climate changes in recent years, there is paramount importance in a detailed investigation of these changes and the prediction of potential future events (Coşkun, 2020a). Temperature and precipitation, as primary climate parameters, exhibit considerable variability spatially and temporally. Data on these parameters significantly contribute to delineating climate characteristics at regional and global scales, aiding in the comprehension of climate changes.

Global temperature increases are forecasted to induce alterations in the hydrological cycle, sea level rise, glacier melt, heightened heat wave frequency and intensity, and more severe droughts. The escalating population accentuates the demand for water, emphasizing the critical role of precipitation. Precipitation, integral to the hydrological cycle, becomes pivotal as decreased

precipitation and elevated temperatures lead to diminished water resources and the onset of droughts.

The impacts of climate change can be scrutinized through trend analysis. Trend analysis, a data analysis method, elucidates the relationship between two or more time-dependent variables using mathematical equations (Terzi & İlker, 2020). This method determines whether meteorological data exhibit increasing or decreasing changes over the years.

Numerous studies on trend analysis exist in the literature. In the Central Anatolia Region, trend analysis of temperature and precipitation data employed the Mann-Kendall and linear trend analysis methods (Kızılelma, Çelik & Karabulut, 2015). The impact of the Recep Yazıcıoğlu Gökpınar Dam Lake in Denizli province on climate was investigated, and trend analysis was conducted using linear regression, Mann-Kendall, and Şen methods (Bacanlı & Tuğrul, 2016). Flow trend analysis in the Yangtze River in China utilized Mann-Kendall and Şen methods (Ali & et al., 2019). In the Eastern Black Sea Basin (Çeribaşı, 2019) and Gümüşhane, Erzincan, and Bayburt provinces (Dalkılıç, 2019), precipitation data underwent trend analysis using Şen, Mann-Kendall, and Spearman's Rho methods. In the Black Sea region, trend analysis of precipitation and temperature parameters was conducted using Mann-Kendall and innovative Şen methods (Tokgöz & Partal, 2020). The coasts of the Aegean Region saw the use of Mann-Kendall and Şen methods for temperature trend analysis (Dün & Gönençgil, 2021), while precipitation and temperature data from the Meriç River Basin underwent similar analysis (Eroğlu, 2021). In Northern Togo, rainfall and temperature data were subjected to trend analysis with

Mann-Kendall and Şen methods (Gadedjisso-Tossou, Adjegan & Kablan, 2021), and in Çankırı and Kastamonu provinces, temperature data were analyzed using Mann-Kendall and Şen methods (İlker & Terzi, 2021). The Asir region of Saudi Arabia underwent rainfall trend analysis through Mann-Kendall family tests, innovative trend analysis, and detrended fluctuation analysis (Mallick & et al., 2021). Trend analysis of precipitation data in a region in India utilized Mann-Kendall and innovative trend analysis (Seenu & Jayakumar, 2021), while temperature data in Muğla underwent analysis with Mann-Kendall and Spearman's Rho methods (Yılmaz, 2021). The Eastern Black Sea Region saw the use of linear regression and modified Mann-Kendall methods for trend analysis of temperature, evaporation, wind, and temperature parameters (Yılmaz, Demir & Sevimli, 2021). Mann-Kendall and innovative Sen trend analyses were employed for precipitation data in Bingöl province (Yükseler, Dursun & Alashan, 2021). The Thrace Peninsula underwent temperature trend analysis using Mann-Kendall, Kendall's Tau, and Şen methods (Eroğlu, 2022). In the Van Lake Basin, temperature trend analysis utilized Mann-Kendall and Şen methods (İrcan & Duman, 2022). Cizre, Şırnak, underwent temperature parameter analysis using Mann-Kendall and Şen trend analysis (Avci, 2023), and precipitation parameter analysis in Elazığ province used Mann-Kendall, Spearman's Rho, and innovative Şen trend analyses (Aydın, 2023). Trend analyses were conducted using Mann-Kendall, Spearman's Rho, and Innovative Şen Trend Method with precipitation and flow data in the Konya Apa Dam Basin (Tuğrul & Hınıs, 2023). The temperature series of Hirfanlı Dam Basin were analyzed by using Mann-Kendall and Sequential Mann-

Kendall Test methods (Zeybekoğlu, 2023). Temporal variation of extreme precipitation in the Konya Closed Basin was investigated using Mann-Kendall, Spearman's Rho and Innovative Şen Trend tests (Köyceğiz & Büyükyıldız, 2019). Using standard duration rainfall intensity data obtained from 207 observation stations in Turkey, the trends of rainfall intensities at the stations were determined with Mann Kendall and Spearman's Rho, while Innovative Trend Analysis methods were used to determine dominance (Zeybekoğlu & Karahan, 2018).

This study delves into the examination of climate change effects in the Ermenek Dam Basin. The alterations in temperature and precipitation data are scrutinized through trend analysis. Linear regression analysis and the Mann-Kendall method are employed for trend analysis, utilizing data from Alanya, Anamur, Karaman, Konya, and Seydişehir stations. Furthermore, the impact of the Ermenek Dam on climate is assessed by analyzing temperature, precipitation, and humidity data both before and after the dam's construction.

Material and method

Material

The Ermenek district is situated at approximately 36°58' north latitude and 32°53' east longitude in the southern part of Anatolia within the Karaman province. Characterized by a mountainous terrain, the district shares borders with the Hadim district of Konya province and the Central district of Karaman province to the north, Anamur district of Mersin province and Gazipaşa district of Antalya province to the south, Gülnar and Mut

districts of Mersin province to the east, and Sarıveliler and Başyayla districts of Karaman province to the west.

The Ermenek Dam, located in the Ermenek district, ranks as the second-highest dam in Turkey and boasts the fourth-largest lake area.

Upon reviewing climate studies, it was deemed more suitable to conduct this study based on the dam basin rather than within the administrative boundaries of the Ermenek district (Figure 1).

Figure 1: Ermenek dam basin

The stations selected for the study included Alanya, Anamur, Ermenek, Karaman, and Mut. However, during the calculation phase, it was noted that the Ermenek station was closed in 2004 and reopened in 2013. Additionally, the Mut station exhibited data deficiencies between 1986 and 1993 and in various periods.

Consequently, Konya and Isparta stations were substituted for Ermenek and Mut stations. Due to the distant location of Isparta province and the availability of continuous data from Seydişehir station, Isparta station was excluded, and data from Seydişehir station were incorporated. The study involved the analysis of data obtained from the General Directorate of Meteorology and State Hydraulic Works spanning the years 1980 to 2021, conducted using the Excel program.

Method

Linear regression analysis

Regression analysis is a statistical method employed to predict the value of a random variable with optimal accuracy based on the values of one or more independent variables [7]. Linear regression is mathematically represented by the equation provided in Equation (1).

$$y = ax + b \tag{1}$$

A positive value of coefficient a signifies an ascending change, a negative value indicates a descending change, and a coefficient value of a that is not significantly distinct from zero suggests no discernible change.

Mann-Kendall method

The Mann-Kendall test, also referred to as Kendall's tau statistic, is a commonly employed technique for identifying trends in hydrometeorological time series (Katipoğlu, Yeşilyurt & Dalkılıç, 2022). Endorsed by the World Meteorological Organization, this nonparametric statistical test method is beneficial as it accommodates missing data and doesn't demand adherence to a

specific distribution for the data (Yu, Zou & Whittemore, 1993; Büyükyıldız & Berktay, 2004).

This test is applied to examine the null hypothesis (H_0) concerning the existence of a trend in a time series. The test statistic is computed using the equation presented in Equation (2).

$$S = \sum_{k=0}^{n-1} \sum_{j=k+1}^{n} sgn(x_j - x_k) \quad (2)$$

$$sgn(x) = \begin{cases} +1 & x > 0 \\ 0 & x = 0 \\ -1 & x < 0 \end{cases}$$

Given in Equation (2) xj and xk are the observed values in years j and k, respectively, and n is the total number of years.

The variance of the test statistic, assuming normally distributed data with a mean of zero, is computed using the equation provided in Equation (3).

$$Var\ (S) = \frac{n(n-1)(2n+5)}{18} \quad (3)$$

If the data in the existing time series are similar, the variance is calculated by Equation (4).

$$Var\ (S) = \frac{n(n-1)(2n+5) - \sum_{i=1}^{r} t_i\ (t_i-1)(2t_i+5)}{18} \quad (4)$$

In the Equation (4), r denotes the number of repeated observations in the data set, ti denotes the number of repeated observations in a series of length i.

After calculating the variance, the Z statistic is determined by Equation (5).

$$Z = \begin{cases} \frac{S-1}{\sqrt{Var\,(S)}} & S > 0 \\ 0 & S = 0 \\ \frac{S+1}{\sqrt{Var\,(S)}} & S < 0 \end{cases} \quad (5)$$

In the two-way test hypothesis at α confidence interval $|Z| \leq Z1-\alpha/2$ the hypothesis is accepted. Otherwise, the hypothesis should be rejected. If the S value is positive, there is an increasing trend, and if it is negative, there is a decreasing trend (Coşkun, 2020b).

Results

Linear regression analysis results

Temperature

Upon examining the Alanya station (Figure 2), it is observed that the annual average temperature ranges from a minimum of 18,2 °C to a maximum of 22,2 °C. The calculated average over 40 years of data is 20 °C. The trend line indicates an upward trend, and the proximity of the average temperature distribution to the linear regression line contributes to the R^2 value of 0.84. Significant fluctuations in temperature, either increases or decreases, are seldom observed at the station. The average temperature difference is 4,0 °C.

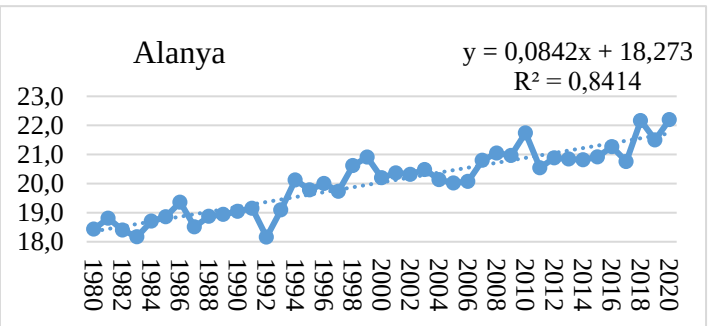

Figure 2: Alanya station temperature linear regression graph

Upon examining the Anamur station (Figure 3), it is observed that the annual average temperature ranges from a minimum of 17,9 °C to a maximum of 21,3 °C. The calculated average over 40 years of data is 19,6 °C. The trend line indicates an upward trend. Deviations from the linear regression line in the mean temperature distribution contribute to the R^2 value of 0.69. Unlike Alanya station, more significant fluctuations in temperature, both increases and decreases, are observed at this station. The average temperature difference is 3,5 °C.

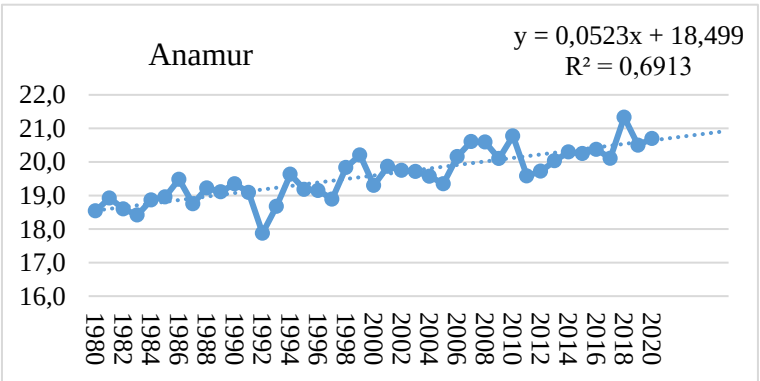

Figure 3: Anamur station temperature linear regression graph

Upon examination of the Karaman station (Figure 4), it is observed that the annual average temperature ranges from a minimum of 9,4 °C to a maximum of 14,8 °C. The calculated average over 40 years of data is 12,2 °C. The trend line indicates an upward trend. Deviations from the linear regression line in the mean temperature distribution contribute to the R^2 value of 0.39. Notably, fluctuations in temperature are recurrent in this station, influenced by the continental climate. The average temperature difference is 5,4 °C.

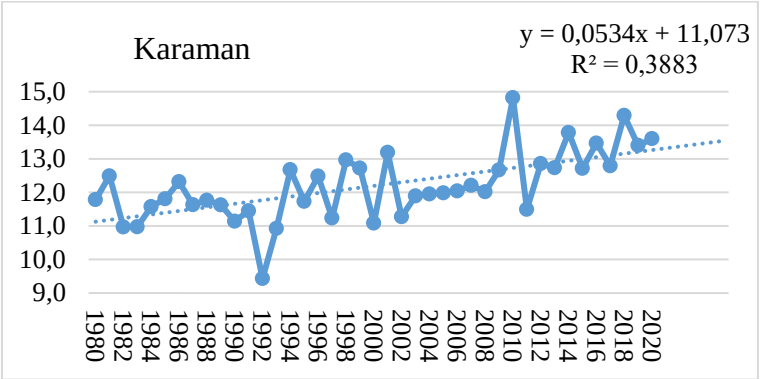

Figure 4: Karaman station temperature linear regression graph

Upon examination of the Konya station (Figure 5), it is noted that the annual average temperature ranges from a minimum of 9,2 °C to a maximum of 15,3 °C. The calculated average over 40 years of data is 12,2 °C. The trend line indicates an upward trend. Deviations from the linear regression line in the mean temperature distribution contribute to the R^2 value of 0.50. Fluctuations in temperature are recurrent in this station, influenced by the continental climate. The average temperature difference is 6,0 °C.

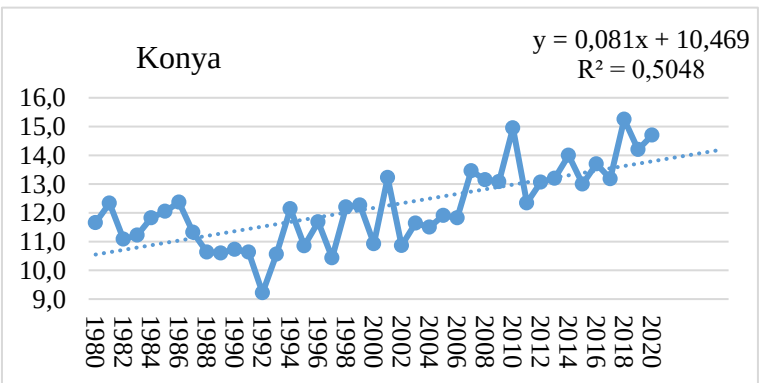

Figure 5: Konya station temperature linear regression graph

Upon examination of the Seydişehir station (Figure 6), it is observed that the annual average temperature ranges from a minimum of 9,6 °C to a maximum of 14,1 °C. The calculated average over 40 years of data is 11,9 °C. The trend line indicates an upward trend. Deviations from the linear regression line in the mean temperature distribution contribute to the R^2 value of 0.33. The station can be considered within the transition climate zone. It is noted that fluctuations are recurrent, and the average temperature difference is 4,5 °C.

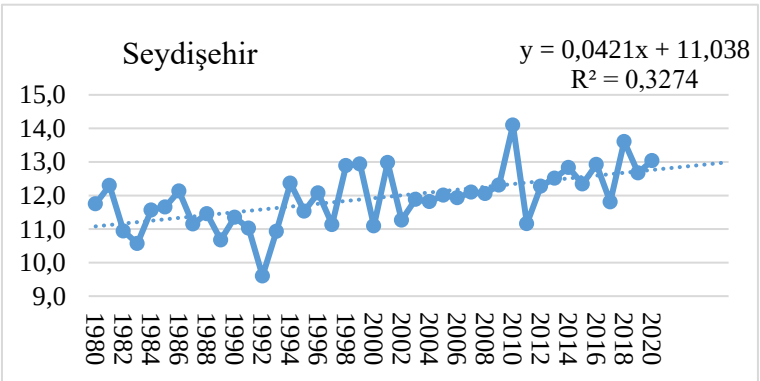

Figure 6: Seydişehir station temperature linear regression graph

Upon analyzing the values from linear regression analysis, it is evident that the trend of temperature increase is anticipated to persist at each station. The trend line in Alanya and Anamur stations aligned with the average value by 1998, whereas Karaman, Konya, and Seydişehir stations reached this level in 2000. As of 2020, Anamur station closely approximates the trend line, while other stations exhibit temperatures above the trend. Predictively, Alanya was forecasted at 21,6 °C, with the actual value at 22,2 °C, resulting in a difference of 0,6 °C. Anamur station was calculated at 20,6 °C,

with the actual value at 20,7 °C, resulting in a minimal difference of 0,1 °C. Karaman station was projected at 13,1 °C, whereas the actual value was 13,6 °C, yielding a difference of 0,5 °C. The calculated value for Konya station was 13,7 °C, while the actual realized temperature averaged at 14,7 °C, resulting in a difference of 1,0 °C. In the analysis of Seydişehir station, the calculated value was 12,7 °C, the actual value was 13,0 °C, and the difference was computed as 0,3 °C. Based on these findings, the lowest increase was 0,1 °C at Anamur station, while the highest increase was 1,0 °C at Konya station.

Precipitation

The annual precipitation at the Alanya station (Figure 7) ranged from a minimum of 623.5 mm=kg/m^2 to a maximum of 1785.6 mm=kg/m^2. The average of 40 years of data was calculated as 1109.6 mm=kg/m^2. Due to the fluctuations in precipitation data at the station, the R^2 value approached zero. Additionally, it is observed that the amount of precipitation is in a decreasing trend.

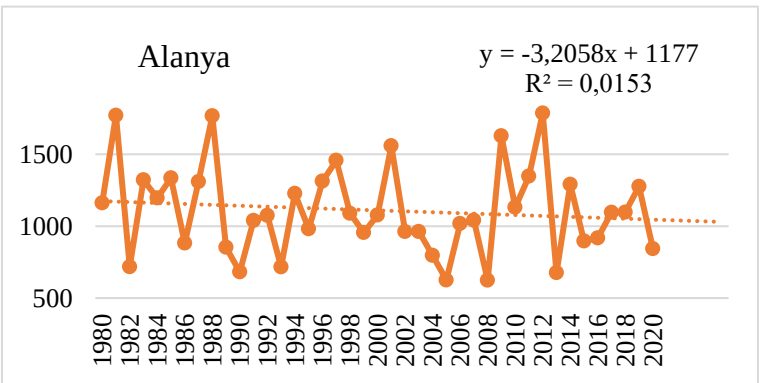

Figure 7: Alanya station precipitation linear regression graph

The annual precipitation at the Anamur station (Figure 8) ranged from a minimum of 447.1 mm=kg/m^2 to a maximum of 1755.1 mm=kg/m^2. The average of 40 years of data was calculated as 912.5 mm=kg/m^2. Due to the fluctuations in precipitation data at the station, the R^2 value approached zero. Additionally, it is observed that the amount of precipitation is in a decreasing trend, albeit very slightly.

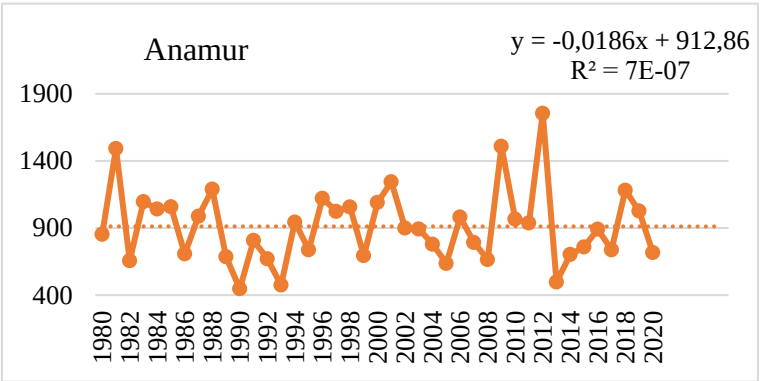

Figure 8: Anamur station precipitation linear regression graph

The annual precipitation at the Karaman station (Figure 9) ranged from a minimum of 220.3 mm=kg/m^2 to a maximum of 802.4 mm=kg/m^2. The average of 40 years of data was calculated as 338.5 mm=kg/m^2. There is less fluctuation in precipitation data at the station compared to Anamur and Alanya stations. In terms of linear regression, it is observed that the amount of precipitation is in an increasing trend.

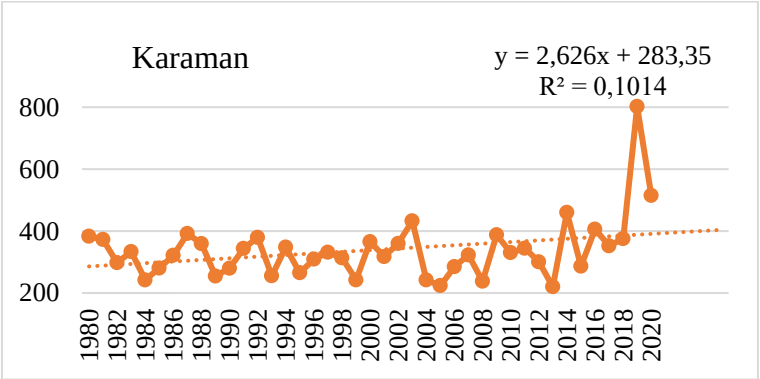

Figure 9: Karaman station precipitation linear regression graph

The annual precipitation at the Konya station (Figure 10) ranged from a minimum of 176.1 mm=kg/m^2 to a maximum of 523.9 mm=kg/m^2. The average of 40 years of data was calculated as 323.8 mm=kg/m^2. Due to fluctuations in precipitation data at the station, the R^2 value approaches zero. In terms of linear regression, it is observed that the amount of precipitation is in a slight increasing trend.

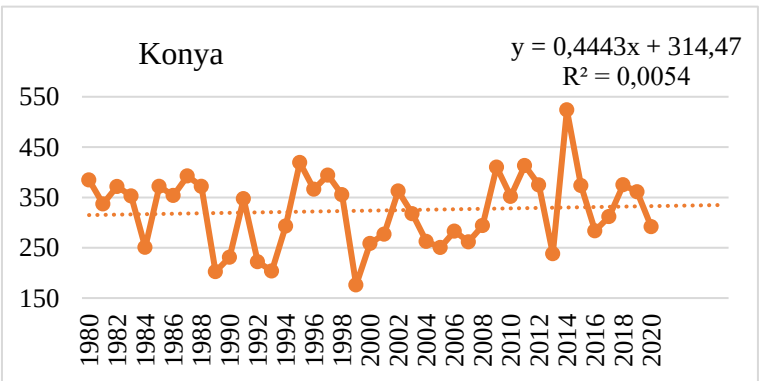

Figure 10: Konya station precipitation linear regression graph

The annual precipitation at Seydişehir station (Figure 11) ranged from a minimum of 474.9 mm=kg/m^2 to a maximum of 1202

mm=kg/m^2. The average of 40 years of data was calculated as 763.9 mm=kg/m^2. Due to fluctuations in precipitation data at the station, the R^2 value approaches zero. In terms of linear regression, it is observed that the amount of precipitation is in a slight increasing trend.

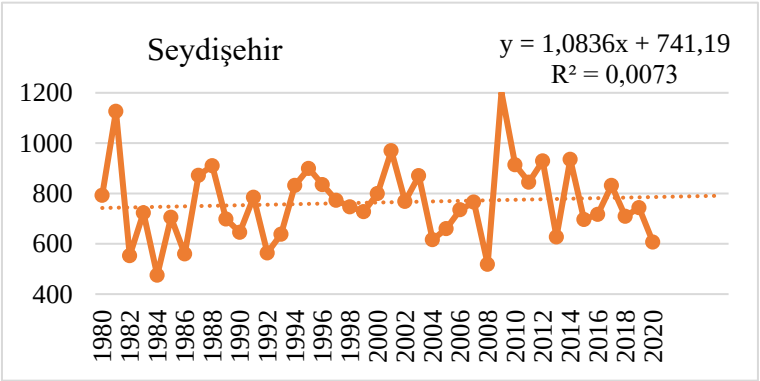

Figure 11: Seydişehir station precipitation linear regression graph

In the linear regression analysis, precipitation exhibits a slight upward trend in regions characterized by continental and transitional climates, whereas it demonstrates a downward trend in regions dominated by the Mediterranean climate.

Mann-Kendall results

Temperature

At Alanya station, it was identified that there is an increasing trend in temperatures during winter, spring, and fall seasons, except for June and July. In June and July, no discernible trend was observed in total and average temperatures during the summer (Table 1).

Table 1: Mann-Kendall method results for Alanya station

	S	VAR	Z	Trend
January	195	7908.33	2.18	+
February	196	7366.67	2.27	+
March	250	7366.67	2.9	+
April	376	7902.00	4.22	+
May	192	7366.67	2.23	+
June	65	7365.67	0.75	
July	88	7366.67	1.01	
August	173	7366.67	1.97	+
September	183	7366.67	2.11	+
October	220	7366.67	2.55	+
November	254	7366.67	2.95	+
December	335	7907.67	3.76	+
Spring	212	7366.67	2.46	+
Summer	82	7366.67	0.94	
Autumn	228	7366.67	2.64	+
Winter	266	7366.67	3.09	+
Total	148	7366.67	1.71	
Average	136	7366.67	1.57	

At the Anamur station, except for January, June, and July, an increasing trend is noted in total and average temperatures during winter, spring, and fall seasons. No distinct trend was observed in temperatures for January, June, and July, as well as during the summer season (Table 2).

Table 2: Mann-Kendall method results for Anamur station

	S	VAR	Z	Trend
January	117	7890.33	1.31	
February	265	7897.67	2.97	+
March	351	7913.00	3.93	+
April	261	7899.67	2.93	+
May	195	7365.67	2.26	+
June	100	7364.67	1.15	
July	116	7364.67	1.34	
August	208	7366.67	2.41	+
September	204	7366.67	2.37	+
October	214	7366.67	2.48	+
November	319	7913.00	3.57	+
December	200	7909.33	2.24	+
Spring	236	7366.67	2.74	+

Summer	124	7366.67	1.43	
Autumn	280	7366.67	3.25	+
Winter	286	7918.00	3.20	+
Total	184	7366.67	2.13	+
Average	176	7366.67	2.04	+

At the Karaman station, excluding January, April, November, and December, there is an observed increasing trend in both average and total temperatures during spring, summer, and fall seasons. Conversely, no significant trend was noted in temperatures for January, April, November, and December, particularly during the winter season (Table 3).

Table 3: Mann-Kendall method results for Karaman station

	S	VAR	Z	Trend
January	29	7921.00	0.31	
February	198	7918.67	2.21	+
March	238	7913.33	2.66	+
April	89	7914.33	0.99	
May	249	7903.00	2.79	+
June	301	7903.00	3.37	+
July	258	7904.67	2.89	+
August	264	7916.64	2.96	+
September	227	7912.33	2.54	+
October	192	7915.33	2.15	+
November	137	7915.00	1.53	
December	58	7916.00	0.64	
Spring	314	7922.67	3.52	+
Summer	266	7366.67	3.09	+
Autumn	320	7915.33	3.59	+
Winter	142	7920.00	1.58	
Total	278	7366.67	3.23	+
Average	276	7364.67	3.20	+

At the Konya station, excluding January, April, November, and December, there is an observed increasing trend in both average and total temperatures during spring, summer, and fall seasons. Conversely, no significant trend was noted in temperatures for

January, April, November, and December, particularly during the winter season (Table 4).

Table 4: Mann-Kendall method results for Konya station

	S	VAR	Z	Trend
January	-8	7920.00	-0.08	
February	179	7908.33	2.00	+
March	196	7920.00	2.19	+
April	65	7919.33	0.72	
May	195	7909.00	2.18	+
June	230	7916.67	2.57	+
July	278	7914.00	3.11	+
August	331	7913.00	3.71	+
September	210	7912.00	2.35	+
October	190	7909.33	2.13	+
November	170	7910.67	1.90	
December	59	7912.33	0.65	
Spring	244	7924.67	2.73	+
Summer	232	7366.67	2.69	+
Autumn	313	7921.67	3.51	+
Winter	134	7924.67	1.49	
Total	214	7366.67	2.48	+
Average	211	7365.67	2.45	+

At the Seydişehir station, an observed increasing trend has been identified in both average and total temperatures during March, July, and August, encompassing the spring, summer, and fall seasons. Conversely, no significant trend was noted in temperatures for other months, including the winter season (Table 5).

Table 5: Mann-Kendall method results for Seydişehir station

	S	VAR	Z	Trend
January	-4	7920.00	-0.03	
February	153	7915.00	1.71	
March	210	7920.67	2.35	+
April	89	7908.33	0.99	
May	170	7910.67	1.90	
June	149	7892.33	1.67	
July	239	7365.67	2.67	+
August	266	7916.00	2.98	+
September	125	7898.33	1.40	

October	107	7909.67	1.19	
November	143	7896.33	1.60	
December	78	7915.33	0.87	
Spring	268	7917.33	3.00	+
Summer	220	7366.67	2.55	+
Autumn	255	7920.00	2.82	+
Winter	144	7924.67	1.67	
Total	348	7926.67	3.90	+
Average	350	7900.00	3.93	+

Upon comprehensive analysis of all stations, a discernible increasing trend is observed across monthly, seasonal, average, and annual total temperatures. Notably, Konya and Karaman stations exhibit similar characteristics and trends.

Precipitation

At the Alanya station, a positive trend was observed solely in September precipitation, while no discernible trend was noted in other months, seasonal assessments, and average and total precipitation data (Table 6).

Table 6: Mann-Kendall method results for Alanya station

	S	VAR	Z	Trend
January	19	7925.67	0.20	
February	-22	7926.67	-0.24	
March	-49	7925.67	-0.54	
April	18	7926.67	0.19	
May	25	7925.67	0.27	
June	-44	7860.00	-0.49	
July	-114	7624.67	-1.51	
August	42	5864.67	0.54	
September	304	7832.67	3.42	+
October	76	7926.67	0.84	
November	-158	7926.67	-1.76	
December	-16	7926.67	-0.17	
Spring	-9	7925.67	-0.09	
Summer	-102	7920.00	-1.13	
Autumn	13	7925.67	0.13	
Winter	28	7926.67	0.30	
Total	-29	7925.67	-0.31	
Average	-29	7925.67	-0.31	

At the Anamur station, a positive trend was observed solely in September precipitation, while no discernible trend was noted in other months, seasonal assessments, and average and total precipitation data (Table 7).

Table 7: Mann-Kendall method results for Anamur station

	S	VAR	Z	Trend
January	61	7925.67	0.67	
February	22	7926.67	0.24	
March	-73	7925.67	-0.81	
April	15	7925.67	0.16	
May	111	7912.33	1.24	
June	-65	7654.33	-0.73	
July	27	4780.33	0.38	
August	67	4783.00	0.95	
September	223	7432.33	2.58	+
October	-89	7925.67	-0.99	
November	-83	7925.67	-0.92	
December	34	7926.67	0.37	
Spring	-44	7926.67	-0.48	
Summer	-31	7858.33	-0.34	
Autumn	-64	7926.67	-0.71	
Winter	154	7366.67	1.78	
Total	-32	7926.67	-0.35	
Average	-32	7926.67	-0.35	

No discernible increasing or decreasing trend was detected at the Karaman station (Table 8).

Table 8: Mann-Kendall method results for Karaman station

	S	VAR	Z	Trend
January	166	7924.67	1.85	
February	-3	7923.67	-0.02	
March	-32	7924.67	-0.35	
April	-62	7924.67	-0.69	
May	-113	7923.67	-1.26	
June	156	7922.67	1.74	
July	-112	7752.00	-1.26	
August	-78	7517.33	-0.20	
September	126	7832.67	1.41	
October	18	7922.00	0.19	
November	-27	7925.67	-0.29	

December	48	7926.67	0.53	
Spring	-88	7924.67	-0.98	
Summer	97	7925.67	1.08	
Autumn	44	7926.67	0.48	
Winter	105	7925.67	1.17	
Total	37	7925.67	0.40	
Average	37	7921.00	0.40	

No discernible trend was observed in precipitation data at Konya station, except for a positive trend identified in September. This observation holds true for other months, seasonal assessments, average, and total precipitation data (Table 9).

Table 9: Mann-Kendall method results for Konya station

	S	VAR	Z	Trend
January	151	7925.67	1.68	
February	-46	7924.67	-0.51	
March	12	7926.67	0.12	
April	-94	7926.67	-1.04	
May	-104	7926.67	-1.16	
June	99	7925.67	1.10	
July	-12	7890.00	-0.12	
August	38	7756.67	0.42	
September	223	7907.00	2.50	+
October	-34	7924.67	-0.37	
November	-79	7925.67	-0.88	
December	48	7926.67	0.53	
Spring	-91	7925.67	-1.01	
Summer	83	7925.67	0.92	
Autumn	-68	7926.67	-0.75	
Winter	62	7926.67	0.69	
Total	38	7926.67	0.42	
Average	35	7921.00	0.38	

No discernible trend was observed in precipitation data at Seydişehir station, except for a positive trend identified in September. This observation holds true for other months, seasonal assessments, average, and total precipitation data (Table 10).

Table 10: Mann-Kendall method results for Seydişehir station

	S	VAR	Z	Trend
January	140	7926.67	1.56	
February	12	7926.67	0.12	
March	24	7926.67	0.26	
April	-13	7925.67	-0.13	
May	50	7926.67	0.55	
June	130	7926.67	1.45	
July	-37	7860.33	-0.41	
August	17	7882.33	0.18	
September	177	7917.00	1.98	+
October	38	7926.67	0.42	
November	-136	7926.67	-1.52	
December	-14	7926.67	-0.15	
Spring	7	7925.67	0.07	
Summer	94	7926.67	1.04	
Autumn	5	7925.67	0.04	
Winter	34	7926.67	0.37	
Total	34	7926.67	0.37	
Average	33	7925.67	0.36	

Comparison of temperature, humidity, and precipitation data before and after the dam

The Ermenek Dam Lake has a water volume of approximately 4.5 billion m3, and the construction of this dam inevitably has environmental implications. It was noted that there was an increase in average temperature values both before and after the construction of the dam (Table 11).

Table 11: Average temperature table before and after the dam

	Before Dam (1965-2004)	After Dam (2013-2018)
January	3.6	4.0
February	3.7	4.3
March	6.3	8.6
April	10.2	10.8
May	14.2	15.0
June	19.7	20.6
July	22.9	23.7
August	22.8	23.3
September	19.3	19.9
October	14.2	15.1
November	8.1	9.3
December	4.6	4.2
Yearly	12.4	13.0

While there is an increase in average temperature, it's noteworthy that the dataset spans 40 years before dam construction, while the post-construction data set covers a 5-year interval. Given that global warming and climate changes are universal phenomena, attributing this increase solely to the dam at this point may be premature. The impact on temperature warrants ongoing investigation.

Dams are known to primarily influence humidity levels. Analyzing Ermenek Dam in terms of humidity reveals that the initial humidity measurements commenced in 1975. These measurements persisted until the closure of the meteorological station in July 2004 and resumed after the station reopened in December 2012. Notably, humidity exhibited the most significant increase during winter months (Table 12).

Table 12: Average humidity table before and after the dam

	Before Dam (1975-2004)	After Dam (2013-2018)
January	58	70
February	57	64
March	52	56
April	47	49
May	44	52
June	38	47
July	32	35
August	33	38
September	37	41
October	43	50
November	53	56
December	57	64
Yearly	46	52

The elevation in humidity values has catalyzed shifts in agricultural practices around the dam. Olive groves have proliferated, and there's been a reduction in fallow land.

Under typical circumstances, precipitation data would be expected to increase; however, a decrease is observed after dam construction (Table 13). Nonetheless, it would be erroneous to directly attribute this to the dam lake. The dataset spans 54 years before dam construction, while there is a post-construction dataset covering 5 years.

Table 13: Average precipitation table before and after the dam

	Before Dam (1950-2004)	After Dam (2013-2018)
January	90.4	75.4
February	67.4	35.8
March	58.7	54.9
April	36.5	22.5
May	33.2	46.7
June	20.5	23.2
July	13.5	2.9
August	8.4	6.9
September	7.6	4.8

October	34.1	40.9
November	63.0	35.6
December	109.3	76.5
Yearly	527.3	425.9

Conclusion

Upon examining the trend analysis, it is evident that temperature values in all stations show an increasing trend in linear regression analysis. Anamur station exhibits the least increase, with 0,1°C, while Konya station displays the highest increase at 1,0°C. Regarding precipitation, Alanya and Anamur stations exhibit a decreasing trend, while the other stations show an increasing trend. Stations with a prevailing continental climate notably exhibit an increasing trend, especially after 2000, attributed to precipitation surpassing the long-term average. Detailed studies using Mann-Kendall trend analysis reveal a positive trend in monthly, seasonal, annual average, and total temperature values, with Karaman and Konya stations exhibiting similar characteristics. Karaman station shows no trend in precipitation, while other stations exhibit a positive trend in September precipitation. This indicates signs of drought in the basin due to increased temperatures and irregularities in the precipitation regime. Although recent precipitation levels have remained consistent, sudden, and short-term precipitation events might result in floods.

Comparing average temperature values before the station's closure and after its reopening in 2013 in the dam region reveals an increase. However, attributing this temperature increase to the dam is deemed premature, given the availability of a 40-year dataset before the dam and only 5 years after its construction. Analyzing precipitation data, a decrease is observed post-dam construction,

contrary to expectations based on factors like surrounding forests and increased humidity. Attributing this decrease solely to the dam is considered inaccurate without considering factors such as the unbalanced dataset, excessive evaporation due to high temperatures, long-term changes in precipitation and flow data, and microclimatic changes induced by the dam. Thus, continuous studies on temperature and precipitation are essential.

Humidity is the parameter undergoing the most rapid change in dam environments, as supported by this study. An increase in humidity measurements between 1975-2004 and 2013-2018 is noted, with the highest increases occurring in winter months and May and June. The rise in humidity during May and June is attributed to warmer weather and the completion of snow melting in the mountains.

Acknowledgement

This study was produced from the doctoral thesis titled 'Investigation of Climate Change Effects in The Ermenek Dam Basin Using Geographic Information Systems and Remote Sensing Techniques' and we thank the General Directorate of Meteorology and the State Hydraulic Works for providing data.

References

Ali, R., Kuriqi, A., Abubaker, S., & Kisi, O. (2019). Long-term trends and seasonality detection of the observed flow in Yangtze River using Mann-Kendall and Sen's innovative trend method. *Water, 11*(9), 1855.

Avci, V. (2023). Cizre'de (Şırnak) aylık ve yıllık ortalama sıcaklıkların eğilim analizi (1963-2021). *Fırat Üniversitesi Sosyal Bilimler Dergisi, 33*(3), 1045-1061.

Aydın, M. (2023). Elâzığ ili yağış verilerinin trend analizi. *Fırat Üniversitesi Mühendislik Bilimleri Dergisi, 35*(1), 159-173.

Bacanlı, Ü. G., & Tuğrul, A. T. (2016). Baraj göllerinin iklimsel etkisi ve Vali Recep Yazıcıoğlu Gökpınar baraj gölü örneği. *Pamukkale Üniversitesi Mühendislik Bilimleri Dergisi, 22*(3), 154-159.

Büyükyıldız, M., & Berktay, A. (2004). Parametrik olmayan testler kullanilarak sakarya havzasi yağişlarinin trend analizi. *Selçuk Üniversitesi Mühendislik, Bilim ve Teknoloji Dergisi, 19*(2), 23-38.

Coşkun, S. (2020a). Aras-Kura kapalı havzasının ortalama sıcaklık, yağış ve akım verilerinin trend analizi (Türkiye). *Fırat Üniversitesi Sosyal Bilimler Dergisi, 30*(2), 29-42.

Coşkun, S. (2020b). Van gölü kapali havzasinda yağişlarin trend analizi. *Mühendislik Bilimleri ve Tasarım Dergisi, 8*(2), 521-532.

Çeribaşı, G. (2019). Şen Yöntemi ve Trend Yöntemleri Kullanılarak Doğu Karadeniz Havzasının Yağış Verilerinin Analiz

Edilmesi. *Journal of the Institute of Science and Technology, 9*(1), 254-264.

Dalkılıç, H. Y. (2019). Yağışların trend analizi. *Erzincan University Journal of Science and Technology, 12*(3), 1537-1549.

Dün, S., & Gönençgil, B. (2021). Ege Bölgesi kıyılarında sıcaklık indislerinin analizi. *Türk Coğrafya Dergisi*, (77), 77-86.

Eroğlu, İ. (2021). Meriç Nehri Havzası'nda sıcaklık ve yağış değerlerinin dönemsel trend analizi. *Avrupa Bilim ve Teknoloji Dergisi*, (23), 750-760.

Eroğlu, İ. (2022). Trakya Yarımadası'nda ortalama hava sıcaklıklarının trend analizi. *Social Sciences Studies Journal, 8*(102), 3121-3144.

Gadedjisso-Tossou, A., Adjegan, K. I., & Kablan, A. K. M. (2021). Rainfall and temperature trend analysis by Mann–Kendall test and significance for Rainfed Cereal Yields in Northern Togo. *Sci, 3*(1), 17.

İlker, A., & Terzi, Ö. (2021). Sıcaklık verilerinin trend analizi: çankırı ve kastamonu örneği. *Mühendislik Bilimleri ve Tasarım Dergisi, 9*(4), 1339-1347.

İrcan, M. R., & Duman, N. (2022). Van Gölü Havzası'ndaki maksimum ve minimum sıcaklıkların trend analizi. *Türk Coğrafya Dergisi*, (80), 39-52.

Kankal, M., & Akçay, F. (2019). Trabzon ili yağışlarının eğilim analizi. *Gümüşhane Üniversitesi Fen Bilimleri Dergisi, 9*(2), 318-331.

Karakuş, C. B., & Güler, Ü. A. (2022). Mann-Kendall trend analizi ile Sivas ilindeki sıcaklık ve yağış trendlerinin belirlenmesi. *Niğde Ömer Halisdemir Üniversitesi Mühendislik Bilimleri Dergisi, 11*(3), 534-544.

Katipoğlu, O. M., Yeşilyurt, S. N., & Dalkılıç, H. Y. (2022). Yeşilırmak havzasındaki hidrolojik kuraklıkların Mann-Kendall ve Yenilikçi Şen yöntemi ile trend analizi. *Gümüşhane Üniversitesi Fen Bilimleri Dergisi, 12*(2), 422-442.

Kızılelma, Y., Çelik, M., & Karabulut, M. (2015). İç Anadolu Bölgesinde sıcaklık ve yağışların trend analizi. *Türk Coğrafya Dergisi*, (64), 1-10.

Köyceğiz, C., & Büyükyıldız, M. (2019). Temporal trend analysis of extreme precipitation: a case study of Konya Closed Basin. *Pamukkale Üniversitesi Mühendislik Bilimleri Dergisi, 25*(8), 956-961.

Mallick, J., Talukdar, S., Alsubih, M., Salam, R., Ahmed, M., Kahla, N. B., & Shamimuzzaman, M. (2021). Analysing the trend of rainfall in Asir region of Saudi Arabia using the family of Mann-Kendall tests, innovative trend analysis, and detrended fluctuation analysis. *Theoretical and Applied Climatology*, 143, 823-841.

Oğuz, E., & Oğuz, K. (2020). Şanlıurfa ili yağış ve sıcaklık trend analizi. *İklim Değişikliği ve Çevre, 5*(1), 13-17.

Seenu, P. Z. & Javakumar, K. V. (2021). Comparative study of innovative trend analysis technique with Mann-Kendall tests for extreme rainfall. *Arabian Journal of Geosciences, 14*(7), 1-15.

Terzi, Ö., & İlker, A. (2020). Kızılırmak Havzası'nda Sıcaklık Değerlerinin Trend Analizi. *Süleyman Demirel Üniversitesi Fen Bilimleri Enstitüsü Dergisi, 24*(3), 626-634.

Tokgöz, S., & Partal, T. (2020). Karadeniz Bölgesinde yıllık yağış ve sıcaklık verilerinin yenilikçi şen ve mann-kendall yöntemleri ile trend analizi. *Journal of the Institute of Science and Technology, 10*(2), 1107-1118.

Tuğrul, T., & Hınıs, M. A. (2023). Konya Apa Barajı Havzasında meteorolojik ve hidrolojik kuraklık trend analizi. *Karaelmas Fen ve Mühendislik Dergisi, 13*(1), 151-163.

Yılmaz, C. B., Demir, V., & Sevimli, M. F. (2021). Doğu Karadeniz Bölgesi meteorolojik parametrelerinin trend analizi. *Avrupa Bilim ve Teknoloji Dergisi,* (24), 489-496.

Yılmaz, A. (2021). Muğla'da sıcaklık verilerinin trend analizi. *Turkish Studies-Social, 16*(5), 1871-1896.

Yu, Y. S., Zou, S., & Whittemore, D. (1993). Non-parametric trend analysis of water quality data of rivers in Kansas. *Journal of Hydrology, 150*(1), 61-80.

Yükseler, U., Dursun, Ö. F., & Alashan, S. (2021). Yağışların mevsimsel değişimlerinin eğilim analiz yöntemleri ile araştırılması: Bingöl ili örneği. *El-Cezeri, 8*(1), 45-59.

Zeybekoğlu, U., & Karahan, H. (2018). Standart süreli yağış şiddetlerinin eğilim analizi yöntemleriyle incelenmesi. *Pamukkale Üniversitesi Mühendislik Bilimleri Dergisi, 24*(6), 974-1004.

Zeybekoğlu, U. (2023). Temperature series analysis of the Hirfanli Dam Basin with the Mann-Kendall and Sequential Mann-Kendall tests. *Turkish Journal of Engineering, 7*(4), 306-313.

CHAPTER IV

Türkiye'deki Ormanlık Alanlardaki 20 Yıllık Değişimin Google Earth Engine ile İzlenmesi: 2001-2021 Analizi

Duygu ARIKAN
Ferruh YILDIZ

1.Giriş

Ekosistemin önemli bir bileşeni olan ormanlar, bitki örtüsünün, toprak ve suyun korunmasında rol oynamaktadır. Uzun dönemler içerisinde doğal ya da antropojenik faaliyetlerin sonucunda ağaçların azalması sonucu, ormansızlaşma meydana gelmektedir (Brovelli, Sun, & Yordanov, 2020; Geist & Lambin, 2001). Ormansızlaşmaya etki eden birçok faktör bulunmaktadır. Örneğin; ekosistem içerisindeki biyoçeşitliliğin azalarak kaybolması, arazinin yanlış kullanımı sonucunda orman, tarım ve toprak erozyonlarının meydana gelmesi, su döngüsünde değişikliklerin yaşanması gibi etkiler ormansızlaşmaya yol açmaktadır (Başaran, 2021; Brovelli et al., 2020; Özdemir, Özkan,

& Mert, 2020). Özellikle gelişmekte olan ülkelerdeki nüfusun artması ve buna bağlı olarak yerleşim alanlarının artarak şehirleşmenin hızlı olması, aynı zamanda ihtiyacı karşılamak amacıyla tarım alanlarını arttırmaya yönelik çalışmalar yapılması doğal sistemi değiştirmektedir (Allen & Barnes, 1985). DeFries, Rudel, Uriarte, and Hansen (2010), yaptıkları çalışmayla orman kayıplarının artmasında, kentsel büyümenin ve aynı bölgedeki tarım alanında yapılan ihracat ile arasında anlamlı ve pozitif bir ilişki olduğunu ortaya koymuşlardır. Orman alanlarındaki değişen durum insan faaliyetlerini, sosyo-ekonomik yapıyı etkilemesinin yanında, ekosistemin işleyişini sağlayan fauna ve florayı da olumsuz olarak etkilemektedir(Brovelli et al., 2020).

Ayrıca, mevsimlerin değişmesi, yıllık yağış miktarındaki düzensizleşmelerin olması, kentsel ve kırsal alanlardaki sıcaklık farklılıkların fazla olmasına yol açmıştır. Bu durum son zamanlarda dünya çapında bir problem haline gelen iklim değişikliklerinin yaşanmasına ve küresel ısınmasının da hızlanmasına sebep olmaktadır. Bu etki nedeniyle aşırı kuraklık, susuzluk gibi faktörlerin etkisiyle ağaçların kuruması ve orman yangınlarının meydana gelmesi de kaçınılmaz olmaktadır. Bu faktörler de orman alanların azalmasına, hatta yok olmasına sebebiyet vermektedir (Arikan & Yildiz, 2023; Oncel Cekim, Güney, Şentürk, Özel, & Özkan, 2021; Tolunay, 2015). Orman alanların azalması sonucunda ağaçlar ve bitkiler tarafından depolanan karbondioksit gazı salınarak, atmosferdeki miktarı artar ve küresel ısınma daha da hızlı gerçekleşir (Seinfeld & Pandis, 2016).

Bu nedenle orman alanlarındaki durumun zamana bağlı olarak incelenmesi ve haritalanması önem arz etmektedir. Uzaktan

algılama ve coğrafi bilgi sistemlerindeki gelişmeler sayesinde yüksek çözünürlüklü uydu görüntülerinin ve verilerin kullanılması ile analiz ve incelemelerin yapılmasına imkân sağlamıştır. Orman alanlarının tespiti ve belirlenmesi çalışmalarında farklı veri türleri, algoritmalar ya da çeşitli bitki indekslerinden yararlanılmaktadır. Yaman and Görmüş (2022), çalışmalarında NDVI (Normalized Difference Vegetation Index- Normalize Edilmiş Fark Bitki Örtüsü İndeksi), EVI (Enhanced Vegetation Index- Gelişmiş Bitki Örtüsü İndeksi), SAVI (Soil-Adjusted Vegetation Index -Toprak Ayarlı Bitki İndeksi), RVI(Ratio Vegetation Index -Oran Bitki İndeksi), TVI(Transformed Difference Vegetation Index -Dönüştürülmüş Bitki İndeksi), NPCRI(Normalized Pigment Chlorophyll Ratio Index -Normalize Pigment Klorofil Oranı İndeks) kullanarak ormana verilen zararı , Arikan and Yildiz (2023), BAI (Burned Area Index- Yanmış Alan İndeksi), NDVI ve SAVI indekslerini orman yangını sonrasında yanan alanı belirlemede, Khunrattanasiri (2023) bölgesel orman alanlarının belirlenmesinde NDVI, SAVI ve GNDVI (Green Normalized Difference Vegetation Index- Yeşil Normalleştirilmiş Fark Bitki Örtüsü İndeksi) gibi çeşitli bitki indekslerinden yararlanılmaktadır. Çalışmalardaki farklı bitki indeksleri, uydularda bulunan bantların kullanılarak matematiksel formülasyonları sonucunda elde edilmiştir. Bu sebepten çalışmada tercih edilen uydunun spektral bantlarının ve özelliklerinin bilinmesi gerekmektedir. Örneğin; Sentinel (ESA), Landsat (NASA) gibi uydu sistemleri çok bantlı iken, EO-1 (NASA), PROBA-1 (ESA) uydular ise hiperspektral bantlıdır.

Ayrıca verilerin işlenmesi, görselleştirilmesi amacıyla kullanılan programlar ve web arayüzleri de geliştirilmektedir.

Bunlardan bir tanesi de Google Earth Engine yazılımıdır. Bulut platformunda işlem yapılabilen, Java ve Python dilinde yazılmış bir web arayüzüdür. İçerisinde bir çok uydu görüntüsünün yanı sıra, çevre, iklim, nüfus gibi verileri barındırmaktadır (Başaran, 2021). Bu yazılım sayesinde literatürde farklı alanlarda yapılmış birçok çalışma bulunmaktadır. Kentsel ve kırsal bölgelerdeki yüzey sıcaklığının incelenmesi (Almeida, Furst, Gonçalves, & Teodoro, 2022; Mohanasundaram, Baghel, Thakur, Udmale, & Shrestha, 2023; Najafzadeh, Mohammadzadeh, Ghorbanian, & Jamali, 2021; Yıldız & Yılmaz, 2022), yangın öncesi ve sonrasındaki alan tahribatının belirlenmesi(İban & Şahin, 2022; Mohammed et al., 2023; Yılmaz, Oruç, Ateş, & Gülgen, 2021), taşkın, sel gibi doğal afetlerin izlenmesi(DeVries et al., 2020; Ghosh, Kumar, & Kumari, 2022; Halder, Das, Bandyopadhyay, & Banik, 2021; Moothedan et al., 2020), atmosferde bulunan kirletici gazların miktarı ve hava kirliliğinin tespiti (Arikan & Yildiz, 2023; Arıkan & Yıldız, 2021; Behera et al., 2021; Huang et al., 2007; Tonion & Pirotti, 2022; Yilmaz, Acar, Sanli, Gulgen, & Ates, 2023), arazi kullanımı ve arazi örtüsündeki değişikliklerin izlenmesi(Aghlmand, Kalkan, Onur, Öztürk, & Ulutak, 2021; Feng et al., 2022; Hu & Dong, 2018; Midekisa et al., 2017), gibi farklı birçok çalışmada GEE yazılımından yararlanılmıştır.

Yapılan bu çalışmada yaklaşık 20 yıllık orman gelişimini ve durumunu değerlendirmek için bulut bilgi işlem hizmeti olan Google Earth Engine (GEE)'den yararlanılmıştır. Bu platform sayesinde hem verilerin analiz edilmesi hem de uydu görüntülerinin indirilmesi sağlanmıştır. Yaşanan değişimin yağış, yüzey sıcaklığı ve NDVI ve EVI (Enhanced Vegetation Index- Gelişmiş Bitki Örtüsü İndeksi)

bitki indeksi ile arasında bir ilişki olup olmadığına bakılmıştır. Ayrıca 2001 ve 2022 yılları içerisindeki EVI bitki indeksi de görsel olarak değerlendirilmiştir. Bu verilerin orman alanlarındaki değişiminde etkili olup olmadığı araştırılmıştır. Bu amaçla makalenin ikinci bölümünde çalışma alanı, verilerin elde edildiği GEE platformu tanıtılmıştır. Ayrıca NDVI ve EVI bitki indeksi hakkında kısaca bilgi verilmiştir. Son bölümde ise, bulgular kısmı yer almakta olup, elde edilen verilerin değerlendirilmesi ve haritalandırılması yapılmış olup, son kısımda tartışma ve sonuçlar ele alınmıştır.

2.Materyal-Metod

2.1.Çalışma Alanı / İş Akış Diyagramı

Çalışma alanı olarak seçilen Türkiye, 36^{o}-42^{o} Kuzey paralelleri ve 26^{o}-45^{o} Doğu meridyenleri arasında yer almaktadır. Gölleriyle birlikte, 783 356 kilometrekare yüzölçümüne sahip ülkenin kuzey kısmında Karadeniz, güneyde Akdeniz, batıda ise Ege denizi ile çevrilidir. Ayrıca, güney batı kısmında iç deniz olarak Marmara denizi bulunmaktadır. Yedi coğrafi bölgeye bölünmüş ve 81 şehir bulunmaktadır. Ülke, iki kıtayı (Avrupa ve Asya) birbirine bağladığından jeopolitik konumu açısından da önem arz etmektedir. Ülkenin doğusu ve batısı arasındaki yükseklik farkının olması, etrafının denizlerle çevrili olması gibi etkenlerden farklı iklim tipleri (karasal, akdeniz, karadeniz) görülmektedir. Bu durum sayesinde de fauna ve flora çeşitliliği de fazla olmaktadır. Ekosistemin %29,4'lük kısmını (22.933.000 ha) orman alanları oluştururken, geriye kalan %70,6'lık (55.071.644 ha) kısmı da yayla, bozkır, kayalık araziler, kum, bataklık, mezarlık, ocak, mera, su alanları, izin verilmiş tesisler vb. alanlarından oluşmaktadır (URL1, OGM).

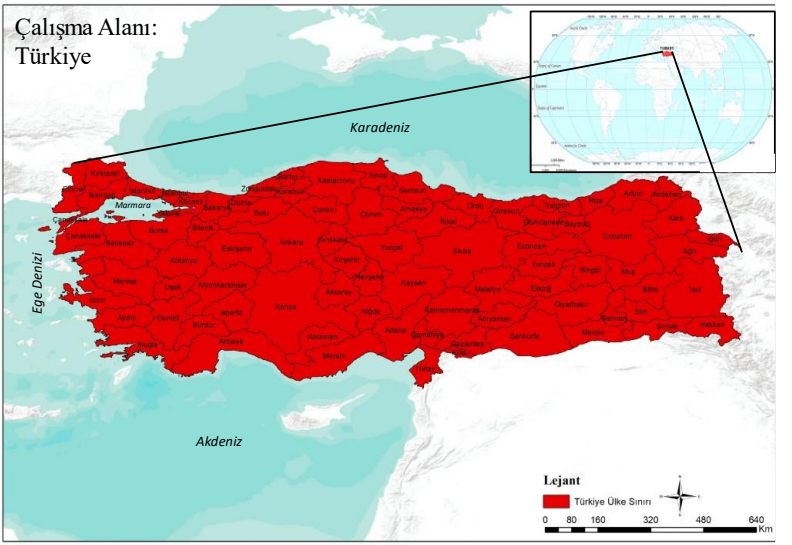

Şekil 1. Çalışma Alanı (Türkiye)

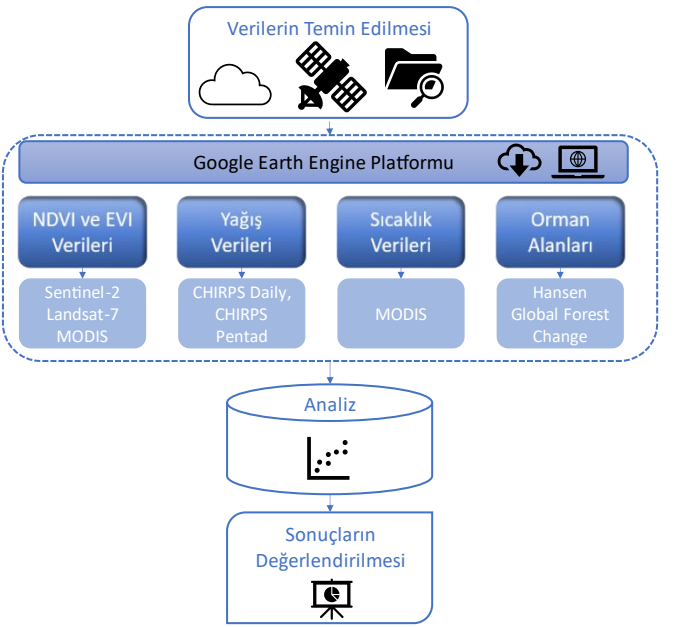

Şekil 2. İş-akış diyagramı

2.2.Kullanılan Veriler

Yapılan bu çalışmada 2001-2022 yılları arasındaki orman durumunu incelemek amacıyla Google Earth Engine kütüphanesinden yararlanılmıştır. Bu kütüphane son yıllarda farklı alanlardaki araştırmacıların modellerini uygulayıp, analiz edebilecekleri ücretsiz bir platform olarak kullanılmaktadır(Brovelli et al., 2020; Campos-Taberner et al., 2018; He et al., 2018; C.-C. Liu, Shieh, Ke, & Wang, 2018). Kullanıcılara açık erişim sağlayan GEE kütüphanesi içerisinde 35 yıldan daha fazla süreyi kapsayan veri arşivi bulunmaktadır (Brovelli et al., 2020). Veri kataloğu içerisinde NASA Landsat uydu misyonu, Avrupa Uzay Ajansı Sentinel uydu misyonu, MODIS, yüksek çözünürlüklü uydu görüntüleri dahil olmak üzere iklim, hava durumu ve atmosferik bilgileri içermektedir (URL1).

Petabayt boyutunda veriye hızlı bir şekilde erişim imkânı bulunmaktadır. Ayrıca veri kütüphanesinin çeşitli olması sayesinde uzaktan algılama çalışmalarında, hastalık salgınlarını tahmin etme, dünya yüzeyindeki değişiklikleri tespit etme, haritalandırmak için kullanışlı bir arayüzü bulunmaktadır. Sistemin yapısı dört panelden oluşmaktadır (Şekil 3). Editör paneli içerisinde Javascript dilinde kodların yazıldığı ve düzenliği kısım yer almaktadır. Aynı panel içerisinde yazılan kodu çalıştırmak ve kaydetmek için de butonlar bulunmaktadır. Yapılan çalışmayı paylaşmak için de koda ait URL bağıntısı aynı panel içerisinde yer almaktadır. Sol panel kısmında Scripts, Docs ve Assests araçları bulunmaktadır. ‘Scripts’ kısmında kullanıcının oluşturduğu kod dosyaları, başka kullanıcılar tarafından oluşturulmuş kodları okumak için ‘reader’ kısmı ve örnek kodların yer aldığı bir alan bulunmaktadır. ‘Docs’ kod düzenleyici

belgelerine ait dosyalarının bulunduğu alan, ‘Assests’ ise dışarıdan yüklenen dosyaların bulunduğu kısımdır. Sağ panelde ise; inspector, console ve tasks diye 3 kısımdan oluşmaktadır. ‘Inspector’ kısmında, çıktı ürünlerinin sorgulandığı bölüm, ‘Console’ kısmında çıktı ürünlerini yazdırmak ve oluşturulan grafikleri göstermek ve son olarak ‘Tasks’ kısmı ise görev yöneticisi olarak çıktı ürünlerini indirmek için kullanılmaktadır. Dördüncü panel ise interaktif harita panelidir. Bu kısımda, oluşturulan tüm harita katmanları ‘Layer’ kısmından bakılabilmektedir. Bu panelin sol kısmında ise, geometrik araçlar ile haritayı yakınlaştırmak ve uzaklaştırmak için araç tuşları bulunmaktadır.

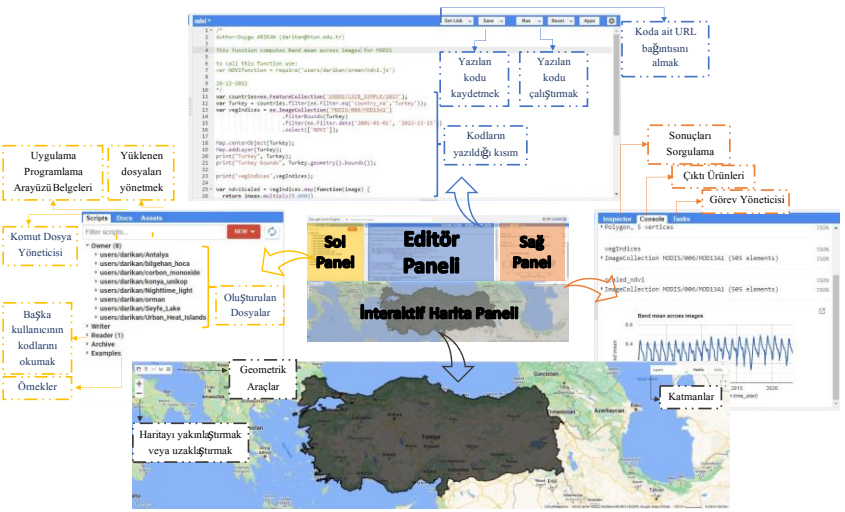

Şekil 3. Google Earth Engine arayüzü (URL3)

Bu çalışmada kullanılan tüm veriler GEE aracılığıyla temin edilmiştir. Şekil 2’ de verilen iş-akış diyagramında kullanılan verilerin ve uyduların isimleri verilmiştir.

Orman alanlarındaki değişikliği izlemek için NDVI ve EVI bitki indekslerinden yararlanılmıştır. Tarımsal verimin izlenmesi, herhangi bir ürünün hasat mevsimi boyunca değerlendirilmesinde, bitki ürünlerinin durumlarını ve süreçlerini karakterize etmek için bu indekslerinden yararlanılmaktadır(Kouadio, Newlands, Davidson, Zhang, & Chipanshi, 2014; H. Q. Liu & Huete, 1995; Rouse, Haas, Schell, & Deering, 1974). Rouse et al. (1974) ve H. Q. Liu and Huete (1995) tarafından bitki örtüsünün spektral imzası yansıtmak amacıyla geliştirilen NDVI ve EVI indekslerinin hesaplanması için formüller Eşitlik 1 ve 2'de sırasıyla verilmiştir. Hem NDVI hem de EVI bitki indeksi 1 ve -1 arasında değerler almaktadır.

$$NDVI = \frac{NIR-RED}{NIR+RED} \qquad \text{(Eşitlik 1)}$$

$$EVI = 2.5 \times \frac{NIR-RED}{NIR+(6\times RED)-(7.5\times BLUE)+1} \qquad \text{(Eşitlik 2)}$$

Eşitlikte verilen *NIR*, yakın kızılötesi kısımdaki (841–876 nm) yansıma, *RED*, kırmızı kısımdaki (620–670 nm) yansıtma ve *BLUE*, mavi kısımdaki (459–759 nm) yansıma değeridir.

Bitki örtüsü çalışmalarında her iki indeks de birbirini tamamlayıcı niteliktedir fakat aralarında küçük farklılıklar bulundurmaktadır. NDVI bitki indeksi daha çok klorofile duyarlı iken, EVI bitki indeksi bitkinin yapısal varyasyonlarına daha duyarlıdır (Schnur, Xie, & Wang, 2010). Fakat, EVI indeksi yüksek biyokütleler için NDVI'dan daha duyarlı olarak görülmektedir(H. Q. Liu & Huete, 1995). Çünkü bu indeks, atmosferdeki ve topraktaki yansıtım değerlerinden daha az etkilenmektedir (H. Q. Liu & Huete, 1995). Ayrıca, bulut, pus ya da sis gibi hava koşullarına karşı EVI daha az etkilenmektedir. Yüksek bitki örtüsü yoğunluğunun

bulunduğu alanlarda EVI daha yüksek hassasiyete sahip olduğu belirlenmiştir(Abbasi et al., 2023; Qin et al., 2023). Bu sebeple yapılan bu çalışmada NDVI indeksine ek olarak EVI indeksi de kullanılmıştır.

3. Bulgular

Yapılan bu çalışmada orman alanlarındaki değişim izlenmiştir. Bu nedenle orman miktarının azalması ya da artması durumuna etki eden sebepler ele alınmıştır. 2001-2022 yılları arasında değişime etki eden faktörlerin zaman serileri oluşturulmuştur. NDVI, bilgisine ulaşabilmek için Sentinel, Landsat ve MODIS uydularından yararlanılmıştır. 2022 NDVI haritasının Sentinel uydu görüntüsünden, 2001 NDVI haritasını Landsat uydu görüntüsünden ve bu yıllar arasındaki NDVI değerlerinin kullanmak amacıyla MODIS uydusu kullanılmıştır. MODIS uydusunun bitki örtüsünü içeren (MOD13Q1) indeksi içerisinde 1.bantta NDVI görüntüsü, 2. bantta ise EVI görüntüsü yer almaktadır.

NDVI haritalarının oluşturulmasındaki temel amacımız, bir bölgenin bitki aktivitesi hakkında yorum yapılabilmesini sağlamaktadır. Şekil 4'te Landsat-7 uydu görüntüsünden elde edilmiş NDVI bitki örtüsünün 2001 yılı, Şekil 5'te, Sentinel-2 uydu görüntüsünden elde edilmiş 2022 yılına ait bitki indeks değerleri sunulmuştur. Farklı uydu kullanılmasındaki temel sebebi, Google Earth Engine platformundaki çeşitliliği göstermek içindir. Ayrıca, mevsimlerin değişmesi bitki indekslerine de etki ettiği varsayılarak hem 2001 yılı için, hem de 2022 yılı için yaz ve kış mevsimlerindeki ortalama indeks değerlerinden oluşturulmuş haritalar da yer almaktadır. 2001 yılının kış mevsimi haritasında kuzey kısmında çok az miktarda veri eksikliği bulunmaktadır.

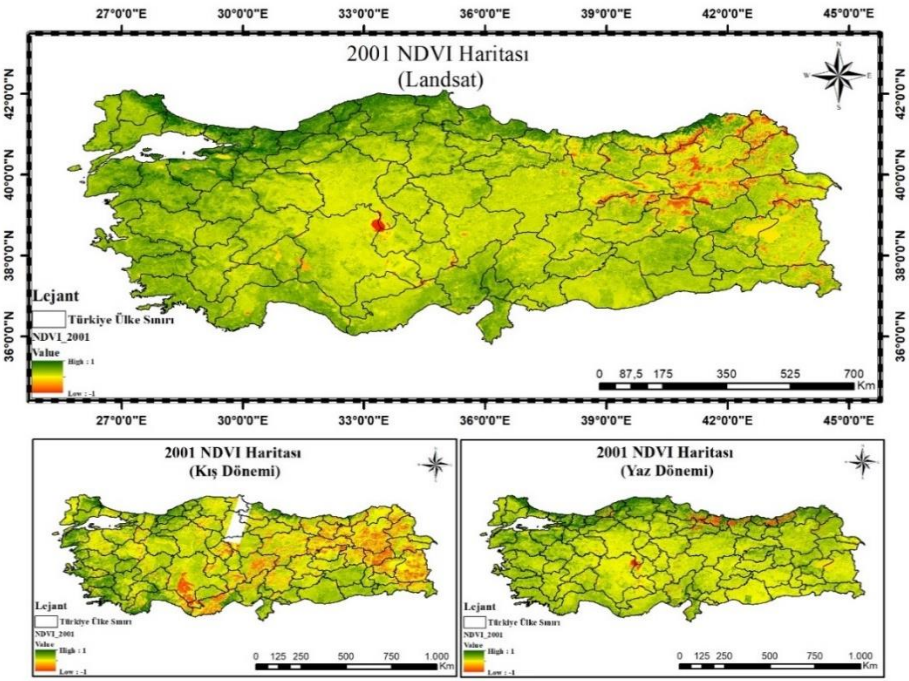

Şekil 2. 2001 yılına ait NDVI haritası

Şekil 4 ve Şekil 5'teki NDVI haritalar yorumlandığında yıllar geçtikçe NDVI değerinde azalmalar olduğu görülmektedir. Genellikle ülkenin kıyı – sahil şeridindeki NDVI yansıtım değerinin iç kesimlere göre daha yüksek olduğu tespit edilmiştir. 2001 yılında Doğu ve Doğu Karadeniz kısımlarında bu değerin düşük olduğu görülürken, 2022 yılında ülkenin genelinde NDVI değeri daha da azalmıştır. Kış dönemindeki indeks değerinin, yaz dönemine göre daha düşüktür.

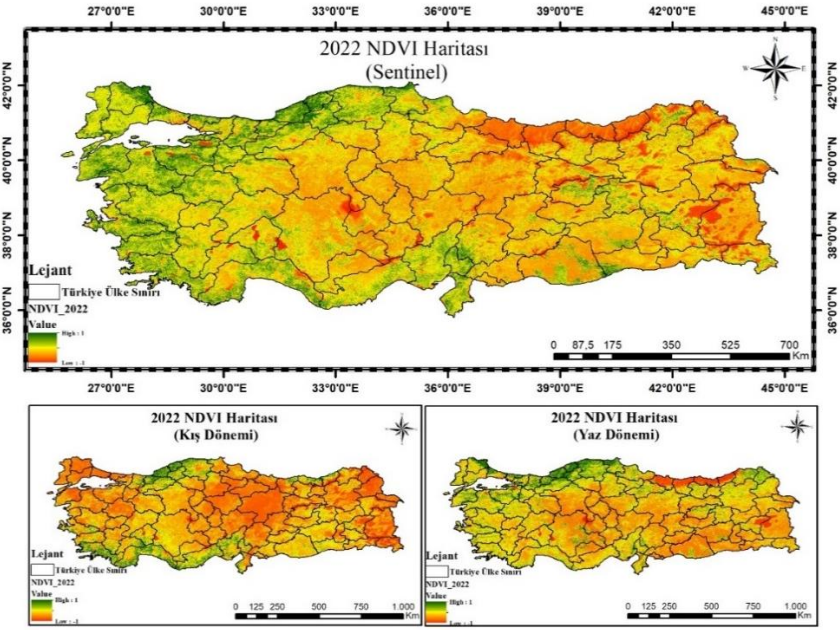

Şekil 3 2022 yılına ait NDVI haritası

Şekil 4 ve Şekil 5'te sadece 2001 ve 2022 yıllarına ait NDVI haritaları görsel olarak sunulmuştur. Diğer yıllardaki durumu daha iyi ifade edebilmek için Şekil 6'da tüm yıllardaki NDVI yansıtım değerleri gösterilmiştir. Bunun için MODIS uydusunun 16 günlük zamansal ve 500 m konumsal çözünürlüğe sahip, NDVI ve EVI kompozitleri kullanılmıştır (URL2). Şekil6'daki grafikten de anlaşılacağı üzere, 2001 yılından 2022 yılına gidildikçe indeks değerinde azalmalar olduğu eğim çizgisinden de görülmektedir. 2001 yılında indeks değeri 0,37 civarında iken 2022 yılında bu değer yaklaşık 0,30'dur. NDVI değerinin maksimum (0,4835) olduğu zaman 2004 yılının mayıs ayı, en minumum (0,1145) olduğu zaman ise 2021 yılının ocak ayıdır. Genellikle kış mevsiminde NDVI değeri düşükken, yaz mevsiminde artış göstermektedir. Şekil 7'de

ise EVI indeksine ait değerler sunulmuştur. Bu grafiğin de NDVI ile uyumlu olduğu görülmektedir. Yani mevsimsel değişimler bitki indekslerinde aynı şekilde yansımıştır.

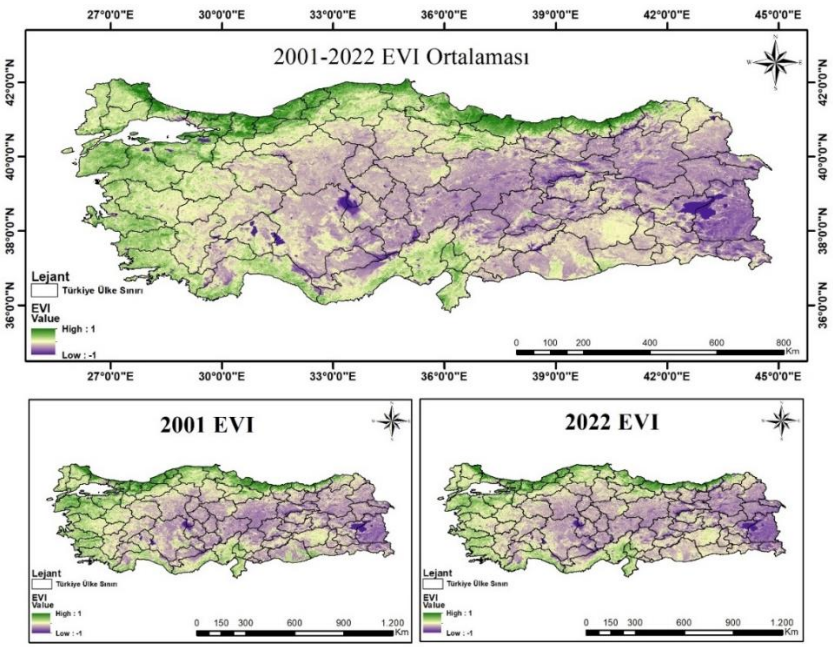

Şekil 4 EVI haritası (2001, 2022)

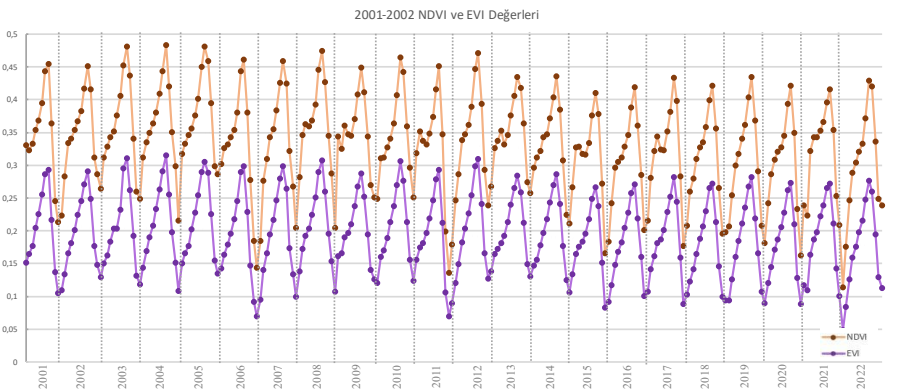

Şekil 5. 2001-2022 yılları arasındaki NDVI ve EVI değerleri

NDVI değerinin yaz ve kış mevsimlerinde farklı olmasından dolayı kara yüzey sıcaklığı ve yağış durumu incelenmiştir. Kara yüzey sıcaklık değerleri için MODIS uydusunun V6.1 ürünü kullanılarak, .csv uzantılı dosyası indirilmiştir. Şekil 7'de, 2001-2022 yılları arasındaki kara yüzey sıcaklığı aylık ortalaması değerleri derece cinsinden ifade edilmiştir. 2022 yılının aralık ayında veri eksikliği olduğu için çalışmaya eklenmemiştir. Kara yüzey sıcaklığının yaz mevsiminde (32^0C-35^0C), kış mevsimine (9^0C-11^0C) göre yüksek olduğu aşikâr bir durumdur. Ortalama değerleri alındığında en düşük sıcaklık ocak ayında, en yüksek sıcaklık da ağustos ayındadır. Tüm yıllar içinde gözlemlenen en yüksek kara yüzey sıcaklığı 2017 temmuz ayında iken, en düşük değer 2006 ocak ayındadır.

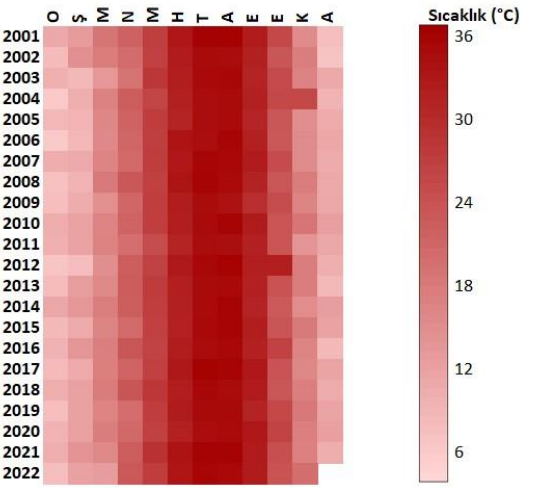

Şekil 6. 2001-2022 yıllarındaki kara yüzey sıcaklığı (ºC)

2001-2021 yılları arasında Türkiye'ye yağan toplam yağış miktarı verilerini elde edebilmek için CHIRPS (Climate Hazards Group Infrared Precipitation with Station) kullanıldı (Funk et al.,

2015). Daha çok çalışmalarda trend analizi ya da mevsimsel kuraklığı izlemek amacıyla 0,05^{o} çözünürlüklü uydu görüntüleri ve istasyon verilerinin birleştirilmesi suretiyle oluşturulmuş veri kaynağıdır. Verilerin indirilmesi Google Earth Engine aracılığıyla sağlanmış olup hem günlük hem de aylık olarak temin edilmiştir. Şekil 8'de aylık düşen yağış miktarı verilmiştir. Her iki veri seti arasındaki yağış miktarı Tablo 1'de ise her iki veri setindeki yağış miktarı ve aralarındaki farklar verilmiştir.

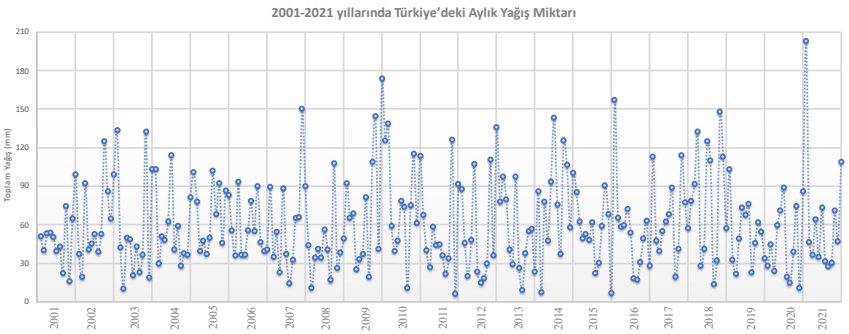

Şekil 7. 2001 -2021 yılları arasındaki Türkiye'deki aylık yağış miktarı

Günlük yağış verilerinin ortalamaları alınmak suretiyle, Türkiye'de en fazla yağış 2018 yılında, en az yağış ise 2008 yılında görülmüştür. 2018 yılındaki değerin maksimum seviyede yüksek çıkmasının temel sebebi Antalya-Kemer bölgesinde ekstrem bir yağış söz konusu olmuştur. Mevsim normalinde yağışların en fazla sonbahar ve kış mevsiminde, en az ise yaz ve ilkbahar mevsiminde olduğu tespit edilmiştir. Tablo 1'deki değerler ele alındığında günlük ve aylık yağış miktarı arasındaki maksimum oluşan fark 10 mm civarındadır.

Tablo 1. CHIRS'den alınan PENTAD ve DAILY arasındaki farklar

Yıllar	***UCSB-CHG/CHIRPS/PENTAD***	***UCSB-CHG/CHIRPS/DAILY***	***Farklar***
2022	515,9297	524,9579	9,0283
2021	662,9313	668,0136	5,0823
2020	571,7751	582,0997	10,3246
2019	768,5552	778,8574	10,3023
2018	791,6344	801,7261	10,0918
2017	629,8081	637,2673	7,4592
2016	625,0654	632,2647	7,1992
2015	644,0108	651,1066	7,0958
2014	694,0870	696,8237	2,7367
2013	647,0213	654,2162	7,1949
2012	758,1790	765,7057	7,5267
2011	658,1559	654,1313	-4,0246
2010	783,3921	793,6146	10,2225
2009	865,6325	876,4206	10,7881
2008	520,6936	527,8370	7,1433
2007	667,8319	674,9768	7,1450
2006	653,3306	660,9111	7,5805
2005	707,6204	713,8588	6,2384
2004	691,4911	701,4049	9,9137
2003	723,1810	728,5842	5,4033
2002	691,3949	698,9488	7,5539
2001	764,8038	772,9247	8,1209

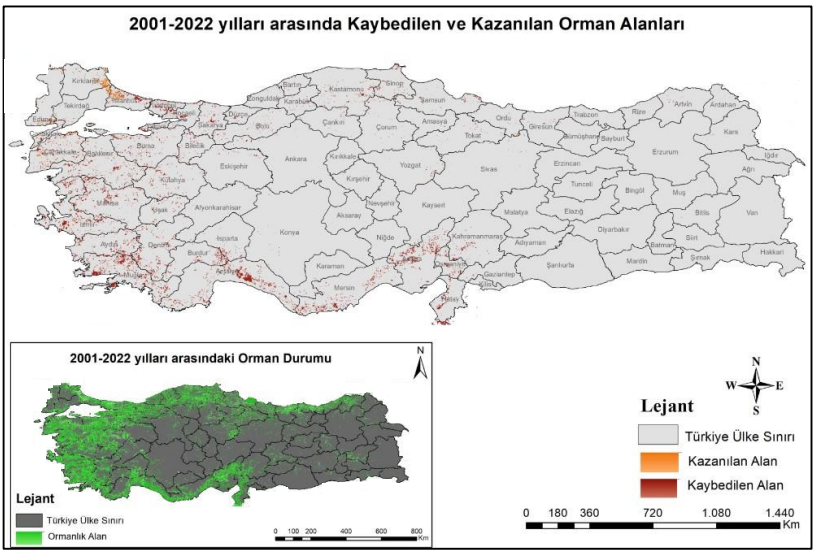

Şekil 8. 2001-2022 yılları arasındaki orman alanlarındaki kazanılan ve kaybedilen alanların haritası

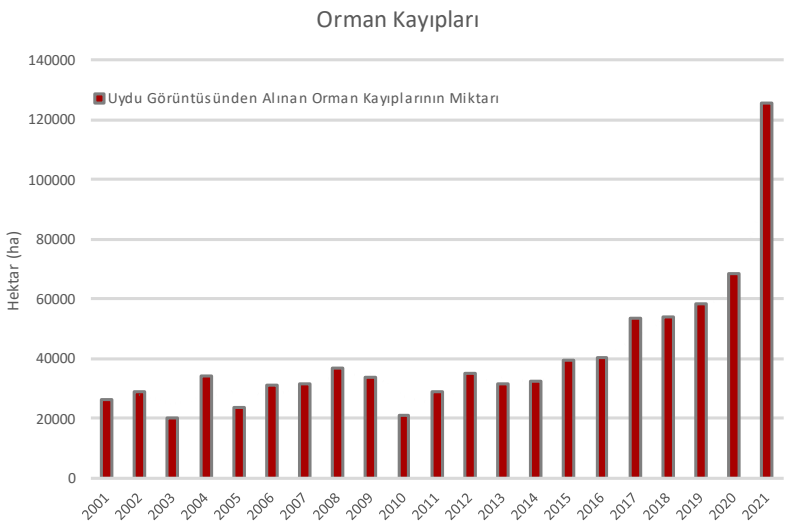

Şekil 9. 2001-2021 yıllarında orman alanlarındaki kayıp miktarı (hektar)

Türkiye' de 2001-2021 yılı içerisinde 125779,03 hektarlık, en çok orman alan kaybının görüldüğü yıl 2021'dir. Türkiye'deki orman varlığının yaklaşık %16,05'lik kısmı 2021 yılında yok olmuştur. Orman Genel Müdürlüğünden aynı yıl içinde yaklaşık %17,08 kadar orman kaybı olduğu belirlenmiştir. Bu da yersel ölçümler ve uzaktan algılama sonucunda elde edilen verilerin tutarlılığını ifade etmektedir.

Orman kayıpları ile NDVI, EVI, sıcaklık ve yağış arasındaki ilişkiye bakılmıştır. Elde edilen sonuçlar doğrultusunda orman yangılarındaki kayıplar sıcaklık ile doğru orantılı, NDVI, EVI ve yağış ile ters orantı olacak şekilde ilişki kurulmuştur (Şekil 12). Son yıllarda sıcaklık miktarının artması ve yağışların azalması orman yangınlarını tetikleyen bir etken olmaktadır. Bu durum da doğrudan orman alanlarının kaybı ile ilişkilendirilebilir. Ayrıca NDVI ve EVI indeksleri arasında %97,03 pozitif yönlü yüksek bir ilişki kurulmaktadır. Her iki indeksinde orman alanlarındaki kayıpla ilişkisi negatif olarak hesaplanmıştır. Çünkü NDVI indeksi, daha çok klorofile duyarlı olup bitkilerin sağlık ve sağlıksız olma durumunu yansıtırken, EVI indeksi de bitkilerin biyokütlesi hakkında bilgi vermektedir. Orman alanlarında kayıp olan yerlerde NDVI ve EVI bitki indeks değerleri düşük olarak tespit edilmiştir.

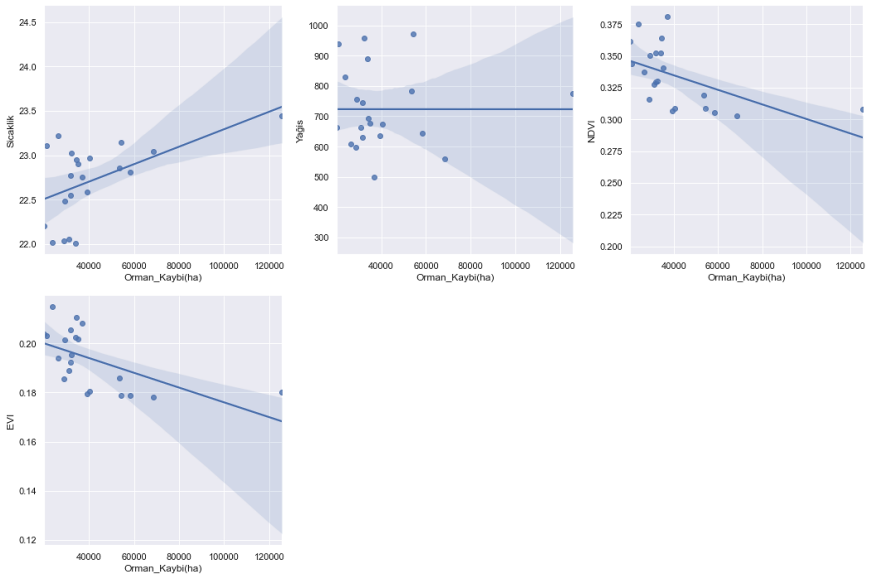

Şekil 10. Orman alanlarındaki kayıp ile Sıcaklık, Yağış, NDVI ve EVI arasındaki ilişki

4. Sonuçlar ve Tartışma

Yeni bir araç olarak kullanılan GEE platformu sayesinde birden fazla uydu görüntüsüne ve veriye bulut üzerinden eş zamanlı bir şekilde erişim imkânı bulunmuştur (Midekisa et al., 2017; Xiong et al., 2017). Ayrıca kullanılan platform sayesinde büyük ölçekteki bir alanın işlemenin kolaylığı görülmüştür.

Yapmış olduğumuz bu çalışmada 2001-2021 yılları arasındaki orman alanlarında değişim zamansal olarak incelenmiş olup, yıllar içerisinde orman alanlarındaki kayıpların arttığı tespit edilmiştir. Çalışma bölgesi için aynı zamanda NDVI, EVI bitki indeksi, sıcaklık ve yağış durumları da incelenmiş olup, aralarında bir ilişki olup olmadığı ortaya konulmuştur. Elde edilen bulgular doğrultusunda son yıllarda yaşanan küresel iklimin etkisiyle sıcaklık

miktarındaki artış ve yağış miktarındaki azalışında orman alanlarında etkisi olduğu tespit edilmiştir. Çünkü, yaz mevsiminde sıcaklık miktarının aşırıl artmasıyla toprak yüzeyinde kuraklık meydana gelmekte ve bu durum da orman yangınlarını tetiklemektedir.

Orman alanlarının miktarının belirlenmesi, değişimin izlenmesi ve araştırılması önem arz etmektedir. Çünkü, insan yaşamının kalitesinde önemli olduğu kadar bitki ve hayvan ekosisteminin sürekliliği ve devamlılığı için önemlidir. Bu amaçla, geleceğe yönelik çalışmalarda alınacak tedbir ya da altlık haritaların oluşturulmasında uydu görüntülerinden yararlanılabileceği, GEE platformunun kullanım kolaylığı bu çalışmada sunulmuştur.

KAYNAKLAR

Abbasi, N., Nouri, H., Didan, K., Barreto-Muñoz, A., Chavoshi Borujeni, S., Opp, C., . . . Siebert, S. (2023). Mapping Vegetation Index-Derived Actual Evapotranspiration across Croplands Using the Google Earth Engine Platform. *Remote Sensing, 15*(4), 1017. doi:https://doi.org/10.3390/rs15041017

Aghlmand, M., Kalkan, K., Onur, M. İ., Öztürk, G., & Ulutak, E. (2021). Google Earth Engine ile arazi kullanımı haritalarının üretimi. *Niğde Ömer Halisdemir Üniversitesi Mühendislik Bilimleri Dergisi, 10*(1), 38-47. doi:https://doi.org/10.28948/ngumuh.795977

Allen, J. C., & Barnes, D. F. (1985). The causes of deforestation in developing countries. *Annals of the association of American Geographers, 75*(2), 163-184. doi:https://doi.org/10.1111/j.1467-8306.1985.tb00079.x

Almeida, C. R. d., Furst, L., Gonçalves, A., & Teodoro, A. C. (2022). Remote Sensing Image-Based Analysis of the Urban Heat Island Effect in Bragança, Portugal. *Environments, 9*(8), 98. doi:https://doi.org/10.3390/environments9080098

Arikan, D., & Yildiz, F. (2023). Investigation of Antalya forest fire's impact on air quality by satellite images using Google earth engine. *Remote Sensing Applications: Society and Environment*, 100922. doi:https://doi.org/10.1016/j.rsase.2023.100922

Arıkan, D., & Yıldız, F. (2021). An Analysis of NO2 Emission During COVID-19 Period in Turkey. *11. Türkiye Ulusal*

Fotogrametri ve Uzaktan Algılama Birliği (TUFUAB) Teknik Sempozyumu, 6-9.

Başaran, N. (2021). *Orman alanları değişimlerinin google earth engine ile incelenmesi: Akdeniz bölgesi örneği.* Eskişehir Teknik Üniversitesi.

Behera, M. D., Mudi, S., Shome, P., Das, P. K., Kumar, S., Joshi, A., . . . Sanwariya, C. (2021). COVID-19 slowdown induced improvement in air quality in India: Rapid assessment using Sentinel-5P TROPOMI data. *Geocarto International*, 1-21. doi:https://doi.org/10.1080/10106049.2021.1993351

Brovelli, M. A., Sun, Y., & Yordanov, V. (2020). Monitoring forest change in the amazon using multi-temporal remote sensing data and machine learning classification on Google Earth Engine. *ISPRS International Journal of Geo-Information, 9*(10), 580. doi:https://doi.org/10.3390/ijgi9100580

Campos-Taberner, M., Moreno-Martínez, Á., García-Haro, F. J., Camps-Valls, G., Robinson, N. P., Kattge, J., & Running, S. W. (2018). Global estimation of biophysical variables from Google Earth Engine platform. *Remote Sensing, 10*(8), 1167. doi:https://doi.org/10.3390/rs10081167

DeFries, R. S., Rudel, T., Uriarte, M., & Hansen, M. (2010). Deforestation driven by urban population growth and agricultural trade in the twenty-first century. *Nature Geoscience, 3*(3), 178-181. doi:http://10.1038/NGEO756

DeVries, B., Huang, C., Armston, J., Huang, W., Jones, J. W., & Lang, M. W. (2020). Rapid and robust monitoring of flood

events using Sentinel-1 and Landsat data on the Google Earth Engine. *Remote Sensing of Environment, 240*, 111664. doi:https://doi.org/10.1016/j.rse.2020.111664

Feng, S., Li, W., Xu, J., Liang, T., Ma, X., Wang, W., & Yu, H. (2022). Land Use/Land Cover Mapping Based on GEE for the Monitoring of Changes in Ecosystem Types in the Upper Yellow River Basin over the Tibetan Plateau. *Remote Sensing*, *14*(21), 5361.

Funk, C., Peterson, P., Landsfeld, M., Pedreros, D., Verdin, J., Shukla, S., . . . Hoell, A. (2015). The climate hazards infrared precipitation with stations—a new environmental record for monitoring extremes. *Scientific data*, *2*(1), 1-21. doi: http://10.1038/sdata.2015.66

Geist, H. J., & Lambin, E. F. (2001). What drives tropical deforestation. *LUCC Report series, 4*, 116.

Ghosh, S., Kumar, D., & Kumari, R. (2022). Cloud-based large-scale data retrieval, mapping, and analysis for land monitoring applications with google earth engine (GEE). *Environmental Challenges, 9*, 100605. doi:https://doi.org/10.1016/j.envc.2022.100605

Halder, B., Das, S., Bandyopadhyay, J., & Banik, P. (2021). The deadliest tropical cyclone 'Amphan': investigate the natural flood inundation over south 24 Parganas using google earth engine. *Safety in Extreme Environments, 3*(1), 63-73. doi:http://doi.org/10.1007/s42797-021-00035-z

He, M., Kimball, J. S., Maneta, M. P., Maxwell, B. D., Moreno, A., Beguería, S., & Wu, X. (2018). Regional crop gross

primary productivity and yield estimation using fused landsat-MODIS data. *Remote Sensing, 10*(3), 372. doi:https://doi.org/10.3390/rs10030372

Hu, Y., & Dong, Y. (2018). An automatic approach for land-change detection and land updates based on integrated NDVI timing analysis and the CVAPS method with GEE support. *ISPRS Journal of photogrammetry and remote sensing, 146*, 347-359. doi:https://doi.org/10.1016/j.isprsjprs.2018.10.008

Huang, J., Minnis, P., Yi, Y., Tang, Q., Wang, X., Hu, Y., . . . Winker, D. (2007). Summer dust aerosols detected from CALIPSO over the Tibetan Plateau. *Geophysical Research Letters, 34*(18). doi: https://doi.org/10.1029/2007GL029938

İban, M. C., & Şahin, E. (2022). Monitoring burn severity and air pollutants in wildfire events using remote sensing data: the case of Mersin wildfires in summer 2021. *Gümüşhane Üniversitesi Fen Bilimleri Dergisi, 12*(2), 487-497. doi:https://doi.org/10.17714/gumusfenbil.1008242

Khunrattanasiri, W. (2023). Application of Remote Sensing Vegetation Indices for Forest Cover Assessments *Concepts and Applications of Remote Sensing in Forestry* (pp. 153-166): Springer.

Kouadio, L., Newlands, N. K., Davidson, A., Zhang, Y., & Chipanshi, A. (2014). Assessing the performance of MODIS NDVI and EVI for seasonal crop yield forecasting at the ecodistrict scale. *Remote Sensing, 6*(10), 10193-10214. doi:https://doi.org/10.3390/rs61010193

Liu, C.-C., Shieh, M.-C., Ke, M.-S., & Wang, K.-H. (2018). Flood prevention and emergency response system powered by Google Earth Engine. *Remote Sensing, 10*(8), 1283. doi:https://doi.org/10.3390/rs10081283

Liu, H. Q., & Huete, A. (1995). A feedback based modification of the NDVI to minimize canopy background and atmospheric noise. *IEEE Transactions on Geoscience and Remote Sensing, 33*(2), 457-465. doi:http://10.1109/TGRS.1995.8746027

Midekisa, A., Holl, F., Savory, D. J., Andrade-Pacheco, R., Gething, P. W., Bennett, A., & Sturrock, H. J. (2017). Mapping land cover change over continental Africa using Landsat and Google Earth Engine cloud computing. *PloS one, 12*(9), e0184926. doi:https://doi.org/10.1371/journal.pone.0184926

Mohammed, Khan, A., Kuri, A., Ahammed, S., Al Muqtadir Abir, K., & Arfin-Khan, M. A. (2023). A google earth engine approach for anthropogenic forest fire assessment with remote sensing data in Rema-Kalenga wildlife sanctuary, Bangladesh. *Geology, Ecology, and Landscapes*, 1-22. doi:https://doi.org/10.1080/24749508.2023.2165297

Mohanasundaram, S., Baghel, T., Thakur, V., Udmale, P., & Shrestha, S. (2023). Reconstructing NDVI and land surface temperature for cloud cover pixels of Landsat-8 images for assessing vegetation health index in the Northeast region of Thailand. *Environmental Monitoring and Assessment, 195*(1), 211. doi:http://doi.org/10.1007/s10661-022-10802-5

Moothedan, A. J., Dhote, P. R., Thakur, P. K., Garg, V., Aggarwal, S., & Mohapatra, M. (2020). *Automatic flood mapping*

using sentinel-1 grd sar images and google earth engine: a case study of Darbhangah, Bihar. Paper presented at the The Proceedings of National Seminar on 'Recent Advances in Geospatial Technology & Applications.

Najafzadeh, F., Mohammadzadeh, A., Ghorbanian, A., & Jamali, S. (2021). Spatial and Temporal Analysis of Surface Urban Heat Island and Thermal Comfort Using Landsat Satellite Images between 1989 and 2019: A Case Study in Tehran. *Remote Sensing, 13*(21), 4469. doi:https://doi.org/10.3390/rs13214469

Oncel Cekim, H., Güney, C. O., Şentürk, Ö., Özel, G., & Özkan, K. (2021). A novel approach for predicting burned forest area. *Natural Hazards, 105*, 2187-2201.

Özdemir, S., Özkan, K., & Mert, A. (2020). Ekolojik Bakış Açısı İle İklim Değişimi Senaryoları. *Biyolojik Çeşitlilik ve Koruma, 13*(3), 361-371. doi:http://doi.org/10.1007/s11069-020-04395-w

Qin, J., Ma, M., Shi, J., Ma, S., Wu, B., & Su, X. (2023). The Time-Lag Effect of Climate Factors on the Forest Enhanced Vegetation Index for Subtropical Humid Areas in China. *International Journal of Environmental Research and Public Health, 20*(1), 799. doi:https://doi.org/10.3390/ijerph20010799

Rouse, J. W., Haas, R. H., Schell, J. A., & Deering, D. W. (1974). Monitoring vegetation systems in the Great Plains with ERTS. *NASA Spec. Publ, 351*(1), 309.

Schnur, M. T., Xie, H., & Wang, X. (2010). Estimating root zone soil moisture at distant sites using MODIS NDVI and EVI in a

semi-arid region of southwestern USA. *Ecological Informatics, 5*(5), 400-409. doi:https://doi.org/10.1016/j.ecoinf.2010.05.001

Seinfeld, J. H., & Pandis, S. N. (2016). *Atmospheric chemistry and physics: from air pollution to climate change*: John Wiley & Sons.

Tolunay, D. (2015). *Türkiye'de Ormansızlaşma İle Kaybedilen Karbon Miktarı.* Paper presented at the 6th National Weather Pollution and Control Symposium.

Tonion, F., & Pirotti, F. (2022). Sentinel-5P NO2 Data: Cross-Validation and Comparison with Ground Measurements. *The International Archives of Photogrammetry, Remote Sensing and Spatial Information Sciences, 43*, 749-756. doi:http://10.5194/isprs-archives-XLIII-B3-2022-749-2022

Xiong, J., Thenkabail, P. S., Gumma, M. K., Teluguntla, P., Poehnelt, J., Congalton, R. G., . . . Thau, D. (2017). Automated cropland mapping of continental Africa using Google Earth Engine cloud computing. *ISPRS Journal of photogrammetry and remote sensing, 126*, 225-244. doi:https://doi.org/10.1016/j.isprsjprs.2017.01.019

Yaman, Ş., & Görmüş, E. T. (2022). Orman Zararlılarının Verdiği Zararın Google Earth Engine Kullanılarak İzlenmesi. *Turkish Journal of Remote Sensing and GIS, 3*(2), 139-149. doi:https://doi.org/10.48123/rsgis.1116907

Yıldız, M. C., & Yılmaz, M. (2022). Yer Yüzeyi Sıcaklığının Google Earth Engine Kullanılarak Elde Edilmesi ve Değerlendirilmesi. *Afyon Kocatepe Üniversitesi Fen Ve Mühendislik*

Bilimleri Dergisi, 22(6), 1380-1387. doi:https://doi.org/10.35414/akufemubid.1181347

Yilmaz, O. S., Acar, U., Sanli, F. B., Gulgen, F., & Ates, A. M. (2023). Mapping burn severity and monitoring CO content in Türkiye's 2021 Wildfires, using Sentinel-2 and Sentinel-5P satellite data on the GEE platform. *Earth Science Informatics*, 1-20. doi:http://10.1007/s12145-023-00933-9

Yılmaz, O. S., Oruç, M. S., Ateş, A. M., & Gülgen, F. (2021). Orman Yangın Şiddetinin Google Earth Engine ve Coğrafi Bilgi Sistemleri Kullanarak Analizi: Hatay-Belen Örneği. *Journal of the Institute of Science and Technology, 11*(2), 1519-1532. doi:https://doi.org/10.21597/jist.817900

URL1: OGM 2020 Türkiye Orman varlığı raporu. https://www.ogm.gov.tr/tr/ormanlarimiz-sitesi/TurkiyeOrmanVarligi/Yayinlar/2020%20T%C3%BCrkiye%20Orman%20Varl%C4%B1%C4%9F%C4%B1.pdf

URL2: https://doi.org/10.5067/MODIS/MOD13A1.061

URL3: https://developers.google.com/earth-engine/tutorials/community/beginners-cookbook


BIDGE